united nations
educational, scientific
and cultural
organization

international atomic
energy agency

the
abdus salam
international centre for theoretical physics

H4.SMR/1150 - 20

Fifth Workshop on Non-Linear Dynamics
and Earthquake Prediction

4 - 22 October 1999

Coupled Evolution of Earthquakes and Faults in a Rheologically Layered Half-Space

Y. Ben-Zion

University of Southern California
Department of Earth Sciences
CA90089-0740 Los Angeles
U.S.A.

EARTHQUAKE CYCLE, FAULT ZONES AND SEISMICITY PATTERNS IN A RHEOLOGICALLY LAYERED LITHOSPHERE

Vladimir Lyakhovsky,[1] Yehuda Ben-Zion,[2] Amotz Agnon[1]

[1]Institute of Earth Sciences, The Hebrew University, Jerusalem, 91904 Israel
[2]Department of Earth Sciences, University of Southern California, Los Angeles, CA 90089-0740, USA

Submitted to JGR, October 1999

ABSTRACT

We study the coupled evolution of earthquakes and faults in a model consisting of a seismogenic upper crust governed by damage rheology over a viscoelastic substrate. The damage rheology has two types of functional coefficients: (1) a "generalized internal friction" separating states associated with material degradation and healing, and (2) damage rate coefficients for positive (degradation) and negative (healing) changes. The evolving damage modifies the effective elastic properties of material in the upper crust as a function of the ongoing deformation. This simulates the creation and healing of fault systems in the upper seismogenic zone. In addition to common vertically averaged thin sheet approximation we introduce a Green function for 3-D elastic half-space for the instantaneous component of deformation. The formulation accounts in an internally consistent manner for evolving deformation fields, evolving fault structures, aseismic energy release, and spatio-temporal seismicity patterns. These developments allow us to simulate long histories of crustal deformation, and to study the simultaneous evolution of regional earthquakes and faults for various model realizations. To focus on basic features of a large strike-slip fault system, we consider first a simplified geometry of the seismogenic crust by prescribing initial conditions consisting of a narrow damage zone in an otherwise damage-free plate. For this configuration, the model generates an earthquake

cycle with distinct inter-, pre-, co-, and post-seismic periods. Model evolution during each period is controlled by a subset of physical properties, which may be constrained by geophysical, geodetic, rock mechanics, and seismological data. In the more generic case with random initial damage distribution, the model generates large crustal faults and subsidiary branches with complex geometries. The simulated statistics depend on the space-time window of the observational domain, i.e.; the model response is non-ergodic. The results indicate that high healing time-scale, τ_h, describing systems with relatively long memory, leads to the development of geometrically regular fault systems and the characteristic frequency-size earthquake distribution. Conversely, low τ_h (relatively short memory) leads to the development of a network of disordered fault systems and the Gutenberg-Richter earthquake statistics. For intermediate values of τ_h the results exhibit alternating overall switching of response, from periods of intense seismic activity and the characteristic earthquake distribution to periods of low seismic activity and the Gutenberg-Richter statistics.

1. Introduction

A decade long surge of activity in the seismological and physics communities is aiming to resolve fundamental questions related to spatio-temporal patterns of earthquakes and faults. Such works employ numerical simulations of models based on different conceptual frameworks. Recent summaries and classifications can be found in e.g., *Gabrielov and Newman* [1994] and *Ben-Zion et al.* [1999a]. Most models to date were confined to studies of seismic activity along a single or a few fault systems. Notable exceptions are the works by *Ward* [1996] and Sornette and co-workers [e.g., *Sornette et al.*, 1994, and references therein], which perform 2-D calculations of elastostatic deformations in a thin plate to simulate, respectively, long histories of regional seismicity and the development of regional faults. Such 2-D models, however, ignore the coupling of the seismogenic zone to other parts of the lithosphere and fault interactions involving the third dimension. The depth plays a major mechanical role through coupling of the upper seismogenic layer to a viscoelastic substrate. This may produce time-dependent inelastic deformation zones that spread in the ductile lower crust and load faults in the brittle upper layer [e.g., *Lehner et al.*, 1981; *Thatcher*, 1983; *Li and Rice*, 1987; *Ben-Zion et al.*, 1993; *Reches et al.*, 1994]. A second important shortcoming of the foregoing models is that they employ either fixed imposed faults [*Ward*, 1996] or material properties that are constant in time [*Sornette et al.*, 1994], and they thus neglect the fact that the geometry and rheological properties of fault systems evolve with the ongoing deformation [e.g., *King*, 1983; *Andrews*, 1989; *Scholz et al.*, 1993]. *Heimpel and Olson* [1996] simulated lithospheric rifting in models with time-independent properties and approximated Elsasser-type interactions (see next section) with the depth dimension. Since stress transfer mechanisms in a 3-D rheologically-layered solid and the evolution of fault properties with deformation can be important over time scales larger than a few great earthquake cycles, the existing models do not provide conceptually complete frameworks for studying long histories of seismic crustal activity.

In the present work we attempt to overcome the above shortcomings by using a model consisting of an elastic upper layer governed by damage rheology [*Lyakhovsky et al.*, 1997a,b]

over a Maxwell viscoelastic substrate. The calculations employ vertically averaged variables of the thin sheet approximation for the viscous component of motion and a 3-D elastic Green function for the elastic response of the model to deformation. Various velocity profiles are imposed as boundary conditions at the base of the viscoelastic lower crust, providing different realizations of mantle drag at the bottom of the lithosheric plates. The damage rheology accounts for the creation, evolution and possible healing of fault zones in the upper crust. The theory of the damage rheology and constraints to damage coefficients from laboratory data are discussed in detail by *Lyakhovsky et al.* [1997a,b] and *Agnon, Lyakhovsky and Ben-Zion* (manuscript in preparation, 1999). In the following, we present theoretical developments relevant to the large-scale structure of the model (layered elastic/viscoelastic half space). The developed framework allows us to simulate long histories of crustal deformation, and to study the simultaneous self-organization of regional earthquake and faults. The model formulation is used to calculate various cases of geodetic fields, evolving upper crust properties, seismicity patterns, and to perform a basic parameter-space study of different dynamic regimes. The results indicate that low healing rate, describing systems with relatively long memory, leads to the development of geometrically regular fault systems, and frequency-size event statistics compatible with the characteristic earthquake distribution. Conversely, high healing rate (relatively short memory) leads to the development of a network of disordered fault systems, and power law frequency-size statistics compatible with the Gutenberg-Richter distribution. The statistics depend on the space-time window of the observational domain, i.e., the response is non-ergodic. For some parameters, the results exhibit alternating overall switching of response, between time intervals of intense and reduced seismic activity.

2. Model Of Crustal Stress Distribution

Strain accumulation and release at a strike-slip plate boundary has been discussed by various authors [e.g., *Sibson*, 1982; *Meisner and Strehlau*, 1982; *Li and Rice*, 1987; *Ben-Zion et al.*, 1993; *Reches et al.*, 1994]. The shallow portion of the lithosphere is generally characterized as elastic and brittle, while the deeper material is assumed to undergo plastic

shear flow and creep due to high temperature and pressure. In this work the seismogenic upper crust is governed by damage rheology and is coupled visco-elastically to the substrate, where steady mantle flow drives the deformation. We use different prescribed loads representing various types of mantle flow, ranging from localized step-function underneath a single major fault to distributed loading for simulations of regional evolutions of earthquakes and faults.

Most studies of surface deformation around a pre-existing plate-boundary (*Li and Rice*, 1987; *Ben-Zion et al.*, 1993; *Reches et al.*, 1994) approximate the velocity profile in the mantle with a step-like function. In these models the mantle on either side of the boundary moves with fixed, opposite polarity, velocity parallel to the major fault. Such a condition assumes that the mantle flow follows the fault trace, although localization in the asthenosphere is not an anticipated feature. Typical simulations of mantle convection do not lead to strong horizontal shear flow localization even in the colder lithosphere.

Elsasser [1969] developed a vertically-averaged thin sheet approximation for a brittle upper crust over a viscous substrate. *Rice* [1980], *Lehner et al.* [1981] and *Li and Rice* [1987] provided a generalized Elsasser model replacing the viscous rheology of the substrate with viscoelasticity. A few attempts have been made to calculate crustal deformation in a 3-D model with a depth dependent rheology [*Ben-Zion et al.*, 1993; *Reches et al.*, 1994]. These simulations used the finite element code ABAQUS and they are very demanding computationally even for modern supercomputers. These results show that outside the space-time vicinity of a large earthquake, the 3-D calculations do not differ much from those obtained by the Elsasser and generalized Elsasser models. *Reches et al.* [1994] presented a direct comparison between a thickness-averaged fault-parallel velocity of the elastic layer from 3-D calculations and the analytical solution of *Li and Rice* [1987] for the generalized Elsasser model. After about 50 years into the earthquake cycle the difference between the 2-D and 3-D models is negligible and at such times both models fit the available geodetic data with about the same accuracy. However, the calculations of *Reches et al.* [1994] and previous results of Rice and coworkers summarized in *Ben-Zion et al.* [1993] show that the generalized Elsasser model is not a satisfactory approximation to deformation in the early part of the earthquake

cycle. In the next section we discuss the main features of the generalized Elsasser model and present a hybrid model incorporating 3-D elastic Green function. The hybrid model provides a good approximation of the deformation field even in spatio-temporal domains close to the occurrence of large earthquakes, while being computationally much more efficient than a fully 3-D model.

2.1 The Generalized Elsasser Model

Figure 1 shows a model consisting of an elastic upper crust governed by damage rheology over a viscoelastic lower crust with imposed basal loading. For a damage free upper crust, the model corresponds to the framework of *Rice* [1980], *Lehner et al.* [1981] and *Li and Rice* [1987]. The horizontal components of a stress tensor σ_{km} averaged over a thickness H of the upper crust are

$$\sigma_{km}(x,y) = \frac{1}{H}\int_{-H}^{0} \sigma_{km}(x,y,z)dz \qquad (1)$$

Substituting (1) into the 3-D equation of equilibrium gives for the crustal stress distribution:

$$\frac{\partial \sigma_{km}}{\partial x_m} = \frac{\tau_k}{H} \qquad (2)$$

where τ_k is shear traction acting at the boundary between the upper and lower crust layers. This shear traction satisfies an equation of motion of the lower crust, which for a Maxwell visco-elastic element is [*Li and Rice,* 1987]:

$$\frac{b}{\mu_a}\frac{\partial \tau_k}{\partial t} + \frac{h}{\eta}\tau_k = \frac{\partial u_k}{\partial t} - V_{plate}^{(k)} \qquad (3)$$

where h, η, and μ_a are thickness, viscosity, and rigidity of the lower crust layer, respectively; $V^{(k)}_{plate}$ is the k-th component of the steady mantle velocity, and b is a scalar discussed below. Expression (3) includes two different terms on the left side. The first describes approximately an instantaneous elastic response of the lower crust to evolving displacement ($\tau_k = \mu_a u_k / b$) and the second corresponds to viscous response of a layer with different velocities on its upper and lower boundaries ($\tau_k = \eta/h \cdot (\partial u_k/\partial t - V^{(k)}_{plate})$). A term $\rho g H \cdot \nabla S$, with ∇S giving the slope of the lower-upper crust interface, should be added to the viscous response if the upper crust has a variable thickness. Such cases are not considered here. The coupled equation of stress distribution, obtained by putting (2) into (3), is

$$\frac{Hb}{\mu_a}\frac{\partial}{\partial t}\frac{\partial \sigma_{km}}{\partial x_m} + \frac{Hh}{\eta}\frac{\partial \sigma_{km}}{\partial x_m} = \frac{\partial u_k}{\partial t} - V^{(k)}_{plate} \qquad (4)$$

Lehner et al. [1981] showed that a vertically averaged stress drop in a homogeneous upper crust governed by (4) gives a displacement similar to a mode III crack in an elastic half space if $b \approx (\pi/4)^2 H$. However, this is associated with an exponential decay of the elastic displacements with distance from the fault, while the exact elastic solution follows an algebraic decay. For long-term deformation the elastic field is only a small perturbation around viscous deformation and the difference between exponential and algebraic decay of the elastic component is not very important. A comparison of deformations generated by an imposed large model earthquake in the generalized Elsasser framework [*Li and Rice*, 1987] and full 3-D simulations [*Reches et al.*, 1994] shows that the former overestimates displacement components having relatively short horizontal wavelengths. However, the difference in thickness-average velocity profile at times larger than tens of years after the earthquake is negligible.

To understand the spatio-temporal evolution of deformation associated with the generalized Elsasser model we analyze the relaxation time of structures with different length scales by using a Fourier decomposition of a 1-D version of (4). We simplify (4) by assuming

that the upper crust obeys Hooke's elasticity and that the deformation field (including imposed plate velocity) has only a "y" component of motion, which depends only on the "x" coordinate (antiplane strain). All material parameters are assumed constant. For these conditions equation (4) reduces to:

$$\frac{Hb\mu}{\mu_a}\frac{\partial}{\partial t}\frac{\partial^2 u}{\partial x^2}+\frac{Hh\mu}{\eta}\frac{\partial^2 u}{\partial x^2}=\frac{\partial u}{\partial t}-V_{plate}^{(k)} \tag{5}$$

For a zero plate motion ($V_{plate}=0$) we look for a basic solution in the form $u(x,t)=f(t)\cdot\varphi(x)$. With this equation (5) becomes:

$$\frac{Hb\mu}{\mu_a}\dot{f}\cdot\varphi''+\frac{Hh\mu}{\eta}f\cdot\varphi''=\dot{f}\cdot\varphi \tag{6}$$

which may be separated into two equations:

$$\frac{\frac{Hb\mu}{\mu_a}\dot{f}+\frac{Hh\mu}{\eta}f}{\dot{f}}=\frac{\varphi}{\varphi''}=-\lambda^2 \tag{7}$$

This procedure gives a basic solution to equation (5) in the form:

$$\varphi=A\cdot\exp\left(i\frac{x}{\lambda}\right)$$

$$f=B\cdot\exp\left(-\frac{hH\mu/\eta}{\lambda^2+bH\mu/\mu_a}t\right). \tag{8}$$

According to this solution, the relaxation time of spatial structure with a horizontal wavelength λ is:

$$t^* = \frac{\lambda^2 + bH\mu/\mu_a}{hH\mu/\eta} \qquad (9)$$

In the short-wave length limit ($\lambda \to 0$) the relaxation time approaches $\frac{bh\eta}{\mu_a}$. For long wave lenghts ($\lambda \to \infty$) we obtain $t^* = \frac{\lambda^2 \eta}{hH\mu}$, which also represents the relaxation time for the original Elsasser model corresponding to b=0. Figure 2 shows how the relaxation time changes as a function of wavelength between these limits. The figure also shows the relaxation time for a new hybrid model described in the next section and used later in our work.

2.2 A Hybrid Model Incorporating 3-D Green Function

As mentioned above, the substitution $\tau_k = \mu_a u_k/b$ essential to the generalized Elsasser model does not reproduce correctly the elastic component of deformation of the lower crust. Our proposed modification of that model follows the usual seismological assumption [e.g., *Kasahara*, 1981; *Stein et al.*, 1994] that the instantaneous response of the earth to a sudden stress redistribution is accommodated by an elastic half space. This assumption is realistic, since the relaxation of strain is not instantaneous even with a lower crust of extremely low viscosity. For example, with a viscosity of 10^{19} Pa s the Maxwell relaxation time is of the order of tens years.

We represent the horizontal displacement field at the boundary between the upper and lower crust layers as a sum of two components: elastic ($u_k^{(e)}$) due to instantaneous deformation in the upper crust, and viscous ($u_k^{(v)}$) due to slow flow in the lower crust:

$$u_k = u_k^{(v)} + u_k^{(e)} \qquad (10)$$

Equating the stress on the both sides of the lower-upper crust interface, the rate of viscous flow is

$$\frac{\partial u_k^{(v)}}{\partial t} = \frac{h}{\eta}\tau_k + V_{plate}^k \qquad (11)$$

For the elastic part of the displacement field we use a 3-D Green function (G_{kn}) in an elastic half space. The elastic displacement at the boundary surface (S) between the lower and upper crust layers is claculated as a convolution of G_{kn} with forces acting at S:

$$u_n^{(e)} = \iint_S G_{kn}\tau_k ds \qquad (12)$$

Taking partial derivative of (12) with respect to time, combining the result with (10) and (11) and substituting back into (2), gives the equation of motion for the hybrid model:

$$H\iint_S G_{kn}\frac{\partial}{\partial t}\frac{\partial \sigma_{nm}}{\partial x_m} ds + \frac{hH}{\eta}\frac{\partial \sigma_{km}}{\partial x_m} = \frac{\partial u_k}{\partial t} - V_{plate}^{(k)} \qquad (13)$$

A strictly rigorous Green function for our calculations would account for the varying topography and varying elastic properties simulated by our model (see section 3), and for the fact that the forces operate at a depth H (=15 km here) below the free surface. However, since we use elsewhere in the model the thin sheet approximation (i.e., vertically-averaged variables), we employ a Green function for a homogeneous elastic half space [*Landau and Lifshitz*, 1970] multiplied by the thickness of the upper layer, instead of precise integration along vertical direction inside the upper crust. The used Green fuction components become

$$G_{xx} = \frac{H}{2\pi\mu_a}\left(\frac{1-\nu}{r} + \frac{\nu x^2}{r^3}\right)$$

$$G_{yy} = \frac{H}{2\pi\mu_s}\left(\frac{1-\nu}{r} + \frac{\nu y^2}{r^3}\right) \qquad (14)$$

$$G_{xy} = \frac{H}{2\pi\mu_s}\frac{\nu xy}{r^3}$$

where r is a radius vector from the origin ($r^2=x^2+y^2$) and ν is Poisson ratio.

Equation (13) differs from equation (4) of the generalized Elsasser model by incorporating a 3-D elastic response to rapid stress variations. Below we refer to the framework described by (13) as a "hybrid model". Similarly to the analysis in the context of equations (4) - (9), we may calculate the relaxation time of spatial structures in the hybrid model with horizontal wave length λ from equation (13) as

$$t^* = \frac{\lambda^2 + H\mu\tilde{G}_{xx}(\lambda)}{hH\mu/\eta}$$

where $\tilde{G}_{xx}(\lambda)$ is the Fourier transformation of the Green function. The solid squares in Fig. 2 show the calculated relaxation time for different wavelengths in the hybrid model incorporating the Green function (14). The relaxation time of this model is similar to that of the generalized Elsasser model for very short length scales, but it approaches the basic Elsasser solution for long wavelengths. The spectral response of the hybrid model, bridging the Elsasser and generalized Elsasser models, corrects the shortcoming of the latter framework associated with overestimation of the lifetime of localized stress anomalies after brittle failures. This shortcoming leads to significant local deviations from 3-D calculations [e.g., *Ben-Zion et al*, 1993; *Reches et al.*, 1994] during the first few years after rapid slip events. This is illustrated in Fig. 3 where we compare fault parallel velocity at two normal distances from the fault as a function of time, calculated with the generalized Elsasser model [eq. A6 from *Li and Rice*, 1987] and our hybrid model.

3. Upper Crust Deformation and Damage Evolution

Our model of a lithosphere, incorporating upper crust material governed by damage rheology over a viscoelastic substrate, can simulate four stages of the seismic cycle: co-seismic, post-seismic, inter-seismic, and pre-seismic deformations. These stages may be anticipated from the behaviour of a viscoelastic degradable composite: a stick-slip behaviour appears if the viscous relaxation time of the non-damaged medium τ_r is longer than the loading time scale τ_L (inverse strain rate) [*Lyakhovsky et al.*, 1997a]. The slip instability corresponds to the co-seismic stage. The inter-seismic stage, spanning most of the stick period, between the post-seismic and pre-seismic stages, is represented by a fast healing and localisation of damage, respectively [*Agnon et al.*, 1999].

The hybrid version of the lithospheric model (Figure 1) generates an earthquake cycle under constant loading. Each element of a two-dimensional horizontal mesh may follow a stick-slip cycle, and the collective behaviour of a group of elements model the faulting process and macroscopic earthquake failure. When deformation in an element reaches a threshold state, damage starts to increase with degradation of elastic moduli and concentration of elastic strain. This spatially localised initial perturbation in strain corresponds to the pre-seismic stage, with small geodetic signals at the free surface (possibly below the typical detection limit). A critical damage level for brittle instability marks the onset of the co-seismic stage during which the local stress drops. This local stress drop may provide a nucleus for rupture that propagates by reloading the adjacent elements to the critical level. The rupture propagation process continues as long as one or more elements experience brittle failure. When no element sustains brittle instability the model earthquake ends. The brittle failure leads to an increase in the cumulative irreversible plastic strain, corresponding to the co-seismic slip in models that idealise the fault-zone as a surface.

The instability during a stress drop requires that we specify the subsequent stress conditions. We allow a full deviatory stress drop under a confining pressure, so the local shear stresses are dropped to zero. This is motivated by earthquake slip hisories infered from observed seismograms [*Heaton*, 1990]; laboratory experiments [e.g. *Brune et al.*, 1993; Anooshehpoor and Brune, 1999]; theoretical models [e.g. *Mora and Place*, 1994; *Andrews and Ben-Zion*, 1997], and a variety of geophysical observations summarized by *Ben-Zion and Andrews* [1998], which suggest that earthquake ruptures propagate in the form of narrow slip pulses associated with strong local dynamic stress drops. The model earthquakes leave the rupture zone under a lithostatic stress condition, favorable for healing of damage in the post-seismic stage which may last from a fraction of a year to a few years, depending on the rate of material recovering. *Agnon et al.* [1999] show the correspondence between a full local stress drop and the rate dependence of friction in experiments.

The imposed plate velocity distribution, length scales for the lithospheric layers, and the rheological coefficients of each layer comprise the parameters of the model. Some of the parameters can be constrained directly from geophysical data. The structural and kinematic values chosen follow a simplified Californian crust with a representative thickness of 35 km [*Fuis and Mooney*, 1990] sheared between plates moving at the surface with differential velocity of 36 mm/yr. Seismic activity is mostly restricted to the upper 10-15 km. We therefore use H=15km and h=20km in the simulation (Figure 1). From seismic refraction and other data [*Fuis and Mooney*, 1990; *Mooney et al.*, 1998], the average rigidity of the crust is estimated at 35-40 GPa for the upper crust and 40-70 GPa for the lower crust and upper mantle. Since the elastic moduli weaken with damage, a reference upper bound of μ=40 GPa is chosen for damage free upper crust rigidity. Below we constrain simulation results with geodetic data to obtain lower crust viscosity (η) and rigidity (μ_a). We also provide additional detail on each stage of deformation evolution, and discuss the role of the remaining parameters. We begin the survey of the parameter space with a simplified model that contains a single straight pre-existing fault zone.

3.1 A Single Fault System

To study the model setting in incremental complexity level we start with a step-like profile of the mantle velocity driving the fault. This profile leads to strain localization and damage evolution in a narrow zone above the step that is set in the center of the model (x=0), while other regions in the crustal model develop no damage. With an appropriate choice of boundary conditions the numerical simulation is required only in a small portion of the space around the fault zone. The interaction of the model region with the outer part of the lithosphere is represented by the boundary conditions at the horizontal edges of the model. Periodic boundary conditions at the edges normal to the fault trace represent infinite repetitions of the fault segment along strike. Conditions at the edges parallel to the fault zone should mimic steady plate motion away from the fault zone. *Andrews* [1978] and *Wdowinski and O'Connel* [1990] give useful discussions of the interaction between fault slip and the chosen boundary conditions. The condition ($V=V_{plate}$ for $x\rightarrow\infty$) may be replaced for a finite model as either (1) constant and uniform fault-parallel velocity ($V=V_{plate}$ for $x=\pm L$), or (2) constant and uniform shear stress (σ_{xy}=const for $x=\pm L$). These seemingly equivalent boundary conditions generate very different solutions for fault-parallel velocity and stress distributions during the inter-seismic period. To illustrate the different behaviour under the two types of boundary conditions, we examine the quasi-static limit appropriate for the long-term ($t\rightarrow\infty$) asymptotic solution by neglecting the temporal derivative on the left hand side of (13). In the case of constant velocity boundary condition, the velocity profile in the model is a straight line ($V(x) = V_{plate} \times x/L$) between zero velocity at the locked fault zone ($V=0$, $x=0$) and plate velocity at the boundary ($V=V_{plate}$, $x=\pm L$). This leads to unbounded increase of stress in the upper crust independently of the viscosity of the lower crust and the rate of motion in the upper mantle. *England and McKenzie* [1982] who used a thin sheet viscous model for the problem of long-term continental deformation assumed a similar decoupling between the plate and the substrate. This "England-Mckenzie loading" does not provide an appropriate description for relatively short-term brittle-elastic behaviour of the upper crust. By contrast, the constant stress boundary condition lead to zero velocity profile and uniform stresses equal

the sum of the stress applied at the boundary and the loading from the mantle. In this case the stress in the model region depends on the viscocity of the lower crust and the rate of motion at the bottom of the model. This "Elsasser loading" [*Elsasser*, 1969] corresponds to a situation where the mantle-crust interaction is an essential part of the crustal processes. Since our simulations include short-term processes of brittle failure in the upper crust, we use the Elsasser loading.

During the inter-seismic period, the damage is approximately frozen and damage evolution does not affect significantly the strain rate of the upper crust. Thus the velocity profile in this period is governed mainly by two model parameters: the imposed mantle velocity and the viscosity of the lower crust. In the following, the mantle velocity is chosen to give far field surface velocity of 1/2 V_{plate} = 18 mm/year, hence long-term slip velocity is 36 mm/year. Fig. 4 shows simulated surface velocity profiles during the inter-seismic stage, 100 years after the last seismic event, for various relaxation times (τ_m) defined as

$$\tau_m = \frac{\pi^2}{16}\frac{H}{h}\frac{\eta}{\mu_a}.$$

The definition of τ_m is based on the solution of the generalized Elsasser model for the elastic layer (eq. 9 with λ=0). The relaxation times used in Fig. 4 are τ_m = 5, 12.5, and 25 years. The lower value corresponds to $\eta = 2.5 \cdot 10^{19}$ Pa s and μ_a = 60 GPa. The intermediate corresponds to $\eta = 5 \cdot 10^{19}$ Pa s and μ_a = 60 GPa, or $\eta = 3 \cdot 10^{19}$ Pa s and μ_a = 40 GPa. The value τ_m=25 years corresponds to $\eta = 10^{20}$ Pa s and μ_a = 60 GPa.

Observed inter seismic fault parallel velocities in geodetic measurements are particularly easy to model in the case where the fault is long and straight and the deformation is uniform in the direction of fault strike. In that case a screw dislocation in an elastic half-space is sufficient to model the observed velocity field at the free surface [*Savage*, 1980] as

$$V = V_0 \frac{1}{\pi} \mathrm{arctg} \frac{x}{D}.$$

This profile, shown in Fig. 4 with a gray line for slip velocity V_0=36 mm/year and dislocation depth D=30 km, provides the best fit [*Savage*, 1990] to inter-seismic geodetic data for the San Andreas Fault in the Transverse Ranges of southern California. *Lisowski* et al. [1991] show that a model with one dislocation fits the geodetic data even better than multi dislocation model. They also show that this fit corresponds to the middle part of the earthquake cycletime T (0.4 - 0.6 T) by comparing with the compiled data of *Thatcher* [1983].

Our model does not produce an exact arctangent velocity profile. Based on the solution of *Chinerry* [1961], the fault parallel elastic component of the displacement (12) with the Green function (14) generated by a stress drop localized along a straight fault, follows an arctangent profile [eq. 4.30 of *Kasahara*, 1981]. The deformation field in our model has additional non-elastic components. Nevertheless, the calculated velocity profiles in Fig. 3 at 100 year after the earthquake (the middle part of simulated 200-year earthquake cycle) are very similar to arctangent curves. As shown in Fig. 1, we consider a model with H=15 km, h= 20 km, and horizontal extent of 150 km x 100 km. The shear modulus and the Poisson ratio of the damage free upper crust material are μ = 40 GPa and ν=0.25, respectively, and Poisson ratio of the lower crust is ν=0.25. We try two different values of the lower crust shear modulus μ_a = 40 and 60 GPa, and three different values of the lower crust viscosity η= 10^{20}, $5 \cdot 10^{19}$, and $2.5 \cdot 10^{19}$ Pa s. The line with τ_m = 12.5 years (η = $5 \cdot 10^{19}$ Pa s, and μ_a = 60 GPa) fits well the geodetic arctangent model. We use these parameters for all simulations to follow.

The inter-seismic period lasts until the current strain diagonality ξ is below a critical value ξ_0 separating states of damage increase (degradation) and decrease (healing) [*Lyakhovsky* et al., 1997a]. This modified internal friction was estimated there to vary between -0.8 and -1.0 using laboratory data on damage onset and laboratory measured internal friction. In the current simulation, ξ_0 together with a prescribed width of the damage zone control the duration of an inter-seismic period, and therefore the length of the earthquake cycle

for a model with a single fault. In this work we use triangular elements of 2.5 km x 2.5 km. This gives a lower bound to the fault zone width in the simulations. Computational limitations prevent us from using a smaller grid size perhaps more appropriate for natural fault zones. A smaller grid size would define the lower magnitude cut-off for the simulated earthquakes, mildly affect our choice of ξ_0, but not the main conclusions of this work. The grid size sensitivity is discussed further below.

Exploratory simulations indicate that for the prescribed 36 mm/yr rate of plate motion and average (effective) lithostatic (confining) pressure $p=(\rho-\rho_w)gH/2=0.1$ GPa (using $\rho=2500$ kg/m^3 and $\rho_w=1000$ kg/m^3), the shear strain in the upper crust never achieves values of ξ_0 inferred from the laboratory data for typical intact crustal rocks. Fig. 5 shows that the change of current strain diagonality ξ with time during the inter-seismic period is very small. After about 100 years ξ is almost constant, and thus small variation in the material property ξ_0 has strong effects. With increase of ξ_0 from -1.40 to -1.35 the length of the cycle increases more than twice, from about 80 years to 190. Further increase of ξ_0 gives even a stronger incremental effect. As shown in Fig. 3 of *Lyakhovsky* et al. [1997a], ξ_0 =-1.35 corresponds to an internal friction of about 0.3 for Poisson ratio equal 0.25. It is reasonable to expect that the value of internal friction characterizing a wide gouge zone in situ with internal cracks (i.e., damage) is smaller that laboratory values associated with small rock samples. Such a low value of friction coefficient is also compatible with the lack of localized frictional heat along the San Andreas fault [e. g., *Brune* et al., 1969, *Lachenbruch and Sass*, 1973]; calculations of changes in seismicity rates [*Simpson and Reasenberg*, 1994] and analysis of aftershock mechanisms [*Zoback and Beroza*, 1993] following the Loma Prieta earthquake; simulated b-values on faults in elastic half-space [Robinson and Benites, 1995]; calculations of stress transfer favoring observed earthquake histories [e. g., *Harris and Simpson*, 1996; *Stein* et al., 1997].

The damage model of brittle material does not include any prescribed surfaces that simulate planar faults. Instead, we have fault zones associated with regions of high damage

having a minimum width equal to a size of one numerical element. While a finite fault zone width is more realistic than a fault surface idealization, the existence of a presribed minimum fault zone width makes some simulation results, like details of the evolving fault zone geometry and minimum model earthquake, dependent on the numerical cell size. This also renders our model inherently discrete in the sense of *Rice* [1993] and *Ben-Zion and Rice* [1995]. The smallest simulated earthquake whose source occupies one element has a vertical size equal to the thickness of the upper crust and should have a magnitude $M \geq 6$. For a given loading and material parameters of the model, this lower cut-off defines an appropriate element size. The isometric cell choice for the simulation, instead of a narrow and elongated one, eliminates any preferred direction related to the numerical procedure. The amount of energy released during a seismic event is proportional to stress drop multiplied by volume of the elements involved in the rupture process. This energy scales linearly with the width of the damage zone. Similarly, the seismic moment of a simulated earthquake and the associated plastic strain (see below) also increase proportionally to the width. The rate of elastic energy accumulation does not depend on the element size, but the energy release rate is proportional to it. Thus, the change of element size leads to proportional change of the duration of the earthquake cycle for a model with a single fault. However, this effect is much weaker than that induced by small changes of the critical strain diagonality and it may be compensated by small variation of ξ_0. The focus of this work is on different possible dynamic regimes of evolving seismicity patterns for a major strike-slip fault system. Since we use the trade-off between fault zone width and ξ_0 to get a realistic average repeat time of large earthquakes, we expect the results on these issues for earthquakes in the approximate magnitude rang $6.0 \leq M \leq 8.5$ not to be affected significantly by the grid size choice.

The inter-seismic period ends and the pre-seismic period begins, when the current strain diagonality achieves a critical value for "subcritical" crack growth. The condition for damage onset ($\xi > \xi_0$) is satisfied and the damage begins to increase. Increasing damage leads to higher strain and further damage localization since the elastic moduli explicitly depend on the damage variable α as discussed by *Lyakhovsky et al.* [1997a]. In addition, for our elastic upper crust governed by damage rheology, the temporal derivative of stress in equation (13 and A4)

includes a term of a type $\frac{\partial\sigma}{\partial\alpha}\frac{d\alpha}{dt}$ that implicitly decreases the effective material stiffness for increasing damage. The process of material weakening and increasing pre-seismic deformation is localized in a small region (one numerical element) and for grid size that represents realistic fault zone width (e.g., order 100 m or less) this "nucleation" process is not expected to produce an observable surface geodetic signal. The pre-seismic period ends when the localized damage achieves a critical value for brittle failure. The duration of this period depends on a damage rate coefficient C_d. This is set here as C_d=0.3-0.5 s^{-1}, a value which is slightly below those (0.5-5 s^{-1}) estimated from laboratory data [*Lyakhovsky et al.*, 1997a] to increase the stability of the numerical procedure. This slightly enlarges the duration of the nucleation weakening period that ends (Fig. 5) with initiation of dynamic rupture when α achieves its critical value ($\alpha=\alpha_{cr}$). At the present modeling level we do not simulate details of the dynamic failure process and use a quasi-static solution. However, we introduce a quasi-dynamic procedure for rupture front propagation by recalculating the stress field after a stress drop in every element involving in the rupture process, and by incorporating a dynamic weakening of material everywhere via reduction of the critical value of the damage parameter to $\alpha_{dynamic}$ given by:

$$\alpha_{dynamic} = \alpha_{CR} - \sqrt{\tau_r \frac{d\alpha}{dt}} \qquad (15)$$

where τ_r is relaxation time given by the ratio of the effective viscosity of the damaged crust to its rigidity. The effective viscosity is moderated by the rate of damage accumulation, yielding τ_r between 10^{-2} and 1-year. Detailed derivation and implications of (15) are discussed in *Agnon, Lyakhovsky and Ben-Zion* [1999]. For infinite viscosity the dynamic weakening (15) implies an ideal brittle behavior. In the initial set of calculations for a single fault model, the parameter τ_r is set unrealistically big, so every nucleation of a brittle failure event in some part of the damage zone propagates through the entire area. This leads to relatively simple failure histories consisting of system-size events occurring in a single fault zone. In the next section we use smaller values of τ_r allowing for the arrest of the rupture front in regions where the

preexisting damage is not high enough. The role of this parameter will be explored further in the next section dealing with distributed faulting.

As mentioned earlier, the brittle failure process is set here to drop initially the deviatoric stresses in the rupture zone to zero, and to conserve only the volumetric stress. This stress drop produces co-seismic displacements in the surrounding material and non-reversible plastic strain in the rupture zone. The latter is modeled in simpler traditional frameworks as slip on a planar fault surface. The amount of plastic strain in the damage zone is related to the total amount of slip-deficit during an earthquake cycle. The magnitude of the simulated earthquake may be estimated from the known stress drop or the accumulated plastic strain. Following *Madariaga* [1979], the tensor of the seismic moment (M_{ij}) is a volumetric integral of the stress drop:

$$M_{ij} = \int_V \Delta\sigma_{ij} dv \qquad (16a)$$

where V is the volume of the zone sustaining the stress drop ($\Delta\sigma_{ij}$). This relation is more general than the usual definition of the seismic moment

$$M_{ij} = \int_V C_{ijkl} \Delta\varepsilon_{kl}^{(plastic)} dv \qquad (16b)$$

where C_{ijkl} is the tensor of elastic moduli. Unfortunately, stress drop determinations are subjected to large uncertainties and it is not possible in practice to obtain $\Delta\sigma_{ij}$ through the failure zone. Another option is to calculate the potency [*Ben-Menahem* and *Singh*, 1981] of the event as

$$P_{ij} = \int_V \Delta\varepsilon_{ij}^{(plastic)} dv \qquad (17)$$

Heaton and Heaton [1989], *Ben-Zion* [1989] and *Amelung and King* [1997] argued that the potency provides a better physical measure of the overall size of an earthquake than the seismic moment. This is because the inclusion of material properties (rigidity) in the definition of the seismic moment makes it ambiguously defined for the general case of laterally heterogeneous fault zones. For simple cases of constant elastic properties, the potency, also referred to as geometric moment [*Kanamori* and *Anderson*, 1975] is equal to the seismic moment divided by rigidity. However, for the more realistic case discussed here, this simple relation does not hold apriori since the elastic properties evolve very strongly during the earthquake rupture process. The relation between moment and potency in our model with variable rigidity is not unique and we analyze it with results based on the distributed damage model of the next section. We calculate the earthquake magnitudes in two ways:

1. From the seismic moment (16a) using the empirical relation M=2/3 ($\log_{10}(M_0)$-16.1), where $M_0 = \sqrt{M_{ij}M_{ij}}$ is in kbar•km^2•cm [*Hanks and Kanamori*, 1979].

2. From the potency using the empirical relation M=(2/3) $\log_{10}(P)$+3.6, where $P = \sqrt{P_{ij}P_{ij}}$ is in km^2•cm [*Ben-Zion and Rice*, 1993].

Figure 6 shows a good correlation between event magnitudes in the model with distributed damage (see next section) calculated in these two different ways. This correlation indicates that a simple linear relation between the moment definition (16a) and potency (17) continues to exist even when the rigidity of the upper crust is variable in space. However, the relation used by seismologists to derive seismic moment from data, (16b) or its Fourier transform, does not have a unique, well-defined meaning for deformation process studied here and presumably occurring during earthquakes involving temporal changes of elastic moduli.

In contrast to rupture nucleation, material healing after the seismic event occurs in the whole rupture zone simultaneously during the post-seismic period. The same term $\frac{\partial\sigma}{\partial\alpha}\frac{d\alpha}{dt}$ that was responsible for stiffness reduction during the pre-seismic period, reverses it sign and locks the damage zone by increasing the effective rigidity. This produces rapid transient strengthening that is followed by actual material healing (i.e., decrease of damage). This temporarily prevents an increase of the strain diagonality during a few years after the event

(Fig. 5) when the damage level is still very high. The characteristic time-scale for material healing depends on values of the coefficients C_1, C_2 in the equation for healing in the damage rheology model [eq. 42 of *Lyakhovsky et al.*, 1997a]. Figure 7 shows the decrease of damage due to confining pressure during three years of the post seismic period for three different pairs (C_1, C_2) used in the simulation and referred to as fast, medium and slow. The material recovers 20-30% of its damage-free rigidity to $\alpha = 0.7 - 0.8$ during the first half a year for all the cases. After that the healing rate significantly decreases and total recovering after three years of the post seismic period approach 30-50% ($\alpha = 0.5 - 0.7$). The period of active locking of the damage zone due to effective stiffness increase and high healing rate is probably of the order of half a year. This time scale is comparable with that reported by *Savage* and *Svarc* [1997] based on post seismic deformation associated with the 1992 Landers earthquakes and by *Zhao et. al* [1997] based on inferred states of stress before and after the 1994 Northridge earthquake. The rate and level of material recovering does not significantly change the behavior of a single fault model, but it governs the style of strain localization and earthquake statistics in the model with distributed faulting discussed in the next section.

3.2 Regional Earthquakes and Fault Networks

The following simulations are aimed to study the process of damage-strain localization, evolution of fault networks, and statistics of simulated seismic events. We start each simulation with randomly distributed damage (and hence stiffness) such that the stress and strain are in equilibrium. Instead of the localized step function velocity of the upper mantle, employed in the previous section, we use a linear velocity profile at the base of the substrate. The values of the base velocities on the left and right edges are equal to those used for the single fault model. All material properties except those responsible for the kinetics of the damage process are the same as in the single fault model.

The ratio between the rate of healing and the rate of loading is central to the model behavior. It controls the style of localization and type of earthquake statistics. We define the

loading time scale, τ_L, as the time needed to re-accumulate (re-build) the elastic shear strain from a stress drop of a brittle failure to a level that gives strain ratio ξ equal to the critical value (ξ_0=-1.35). This loading time scale depends on the relaxation time of the visco-elastic system of upper and lower crust layer (Fig. 2), and the amplitude of the imposed mantle motion. The healing time scale, τ_h, characterizes the rock memory, or how long a material that is broken in a seismic event stay significantly weaker than its unbroken surrounding. This value depends on confining pressure and healing rate coefficients (Fig. 7). In the following set of simulations we keep the loading time scale constant and vary the healing rate coefficients.

The first set of simulations corresponds to slow healing (solid line in Fig. 7). The geometry of the high damage zone formed by the few first events reflects the initial random distribution and keeps its overall geometrical features during more than a thousand model years. Most of the seismic events occur in the same zone and occupy a similar volume. The slip accumulates in a relatively narrow and regular damage zone (Fig. 8a) and preserves some features of the initial random damage for a long period (Fig. 8b). This behavior leads to a preferred event size manifested as a narrow local maximum in non-cumulative frequency-size statistics of model earthquakes. We refer here to such statistics with a preferred event size as characteristic earthquake distribution. The magnitude of the characteristic events strongly depends on the prescribed dynamic weakening. Relatively small values (τ_r=0.1 year) give a maximum in the non-cumulative statistics for earthquakes with magnitude from 6.7 to 6.9 (Fig. 9). Relatively large values of the dynamic weakening (τ_r=0.3 year) shift the maximum to event magnitude of about 7.2 - 7.4 without changing the form of the statistics. Synthetic event catalogs of different length gives the same form of statistics so in this case the process appears to be stationary in time.

Increasing of the material recovering (dash line in Fig. 7) leads to broadening of the maximum in the non-cumulative frequency-size statistics (Fig. 10) changing it towards a Gutenberg-Richter power law distribution. The cumulative number of events with magnitude larger 7.2 could be approximated by a linear relation with b=2.5, a value significantly larger than the observed b-value near unity. Further increasing of the material recovering (dot line in

Fig. 7) significantly increases the geometrical complexity of the evolving damage zones (Fig. 11). The large conjugate structures accumulate significant amount of displacement (Fig. 11a). The offset between fault segments increase and some of them produce branching that prohibits their further propagation. Part of the simulated region could preserve distributed damage (Fig. 11b) without being involved in the process of damage localization during a long time. The frequency-size earthquake statistics for the fast healing case are much closer to the Gutenberg-Richter distribution. A linear relation with b=1.3 could approximate the cumulative statistics of events with magnitude larger 6.8 (Fig. 12). If the crust properties other than damage are homogeneous, the geometrical complexity of the fault system (Fig. 11) is not preserved during a period of several earthquake cycles. In this case a broad damage zone has a tendency to collapse into a narrow one similar to that shown in Fig. 8 sustaining characteristic earthquakes that produce deviation from the Gutenberg-Richter distribution for events with magnitude 7.0-7.3. The situation is, however, different for slightly heterogeneous crust. Even small spatial variations in material parameters representing the strength of the upper crust as critical strain diagonality (ξ_0), or dynamic weakening (τ_d), or both, prevent this regularization tendency and lead to fault zones with sustained geometrical complexities. The corresponding earthquake statistics follows the Gutenberg-Richter distribution with b=1.3 (Fig. 13) for the entire simulated magnitude range.

In such cases, the temporal evolution of seismicity (Fig. 14) is not stationary and produces a particular form of clustering that we have called "mode switching" activity [*Ben-Zion et al.*, 1999b]. There are periods of high seismic activity with several very strong events and series of events induced by a strong one. Most of the earthquakes have magnitudes above 6.8, while during the quiet periods the event magnitudes are below this level. A cluster of strong events with magnitudes between 7-7.5 (insert A) and series of events mimic narrow (insert B) and wide (insert C) fore- and after-shock series surrounds the events with magnitude above 8. In addition to earthquake cycles, there is longer period cycling of high and low seismic activity. This implies that different statistical models should describe the system during different modes of activity, and that the system exhibits strong non-ergodic features.

4. Discussion

We introduce a nonlinear-continuum-mechanics framework for simulating the coupled evolution of earthquakes and faults in a regional model consisting of a seismogenic upper crust governed by damage rheology over a layered viscoelastic half-space. The damage rheology [*Lyakhovsky et al.*, 1997a] incorporates nonlinear and irreversible aspects of rock deformation, including localization and nucleation phases, strength evolution with slip and time, and branching from the main rupture plane. The model accounts for interactions between evolving fault zones, and interaction of the brittle seismogenic crust with a viscoelastic substrate. The results illustrate the importance of four different time scales on the evolution of the crust and frequency-size earthquake statistics.

Our previous analyses [*Lyakhovsky et al.*, 1997a; *Agnon et al.*, 1999] focused on three of the controlling time scales. One for degradation, τ_d, is the inverse of the modulus degradation rate and characterises the duration of the period between damage onset and brittle failure. The second one for loading, τ_L, is the inverse of the total strain-rate and characterises the time needed to re-accumulate the elastic strain from a stress drop of a brittle failure to a level that gives the damage onset. The duration of the earthquake cycle in the single fault model is equal to the sum of τ_d and τ_L. The third time scale, τ_r, comes from the Maxwell relaxation of elastic stresses and is equal to the viscosity divided by rigidity. The dynamic weakening (15) depends on the value of τ_r and thus controls the preferred event size for the characteristic frequency-size distribution. The present work highlights the role of an additional time scale, the healing time τ_h, controlling fault-pattern evolution and earthquake statistics in the model for the crust-mantle system (see also Ben-Zion et al. [1999b]).

Lyakhovsky et al. [1997a] show a stick-slip cycle with three stages: degradation, instability, and healing. These stages correspond to the inter-seismic, co-seismic, and post-seismic stages of a seismic cycle, respectively. The existence of a forth stage – pre-seismic – is indicated by the analysis of localisation in a degradable and purely elastic

one-dimensional material [*Lyakhovsky et al.*, 1997a]. The localisation is also anticipated in a degradable viscoelastic medium if the loading is faster than the viscous relaxation of elastic stress in the undamaged medium ($\tau_r > \tau_L$). *Agnon et al.* [1999] further show that once the degradation is faster than the relaxation ($\tau_r > \tau_d$) the pre-seismic equivalent stage of sub-critical crack growth is terminated and a dynamic stress drop ensues. These results are similar to a transition from quasi-static nucleation phase to dynamic rupture in rate- and state-dependent [e.g., *Okubo*, 1989; *Dieterich*, 1992; *Ben-Zion and Rice*, 1997] and slip weakening [*Shibazaki and Matsu'ura*, 1992; *Ohnaka*, 1996] frictional frameworks.

The full four stages in the seismic cycle are manifested in the present model, incorporating the elastic response of a 3-D half-space. The model provides an improvement over the generalised Elsasser model [*Li and Rice*, 1987] in simulating geodetic signals with algebraic decay compatible with observations, close to the fault as well as in the far field. The calculated velocity profile for the fault parallel velocity fits well an arctangent curve (Fig.4) that represents the average geodetic measurements for the middle part of the earthquake cycle, all the way to the fault zone. During the pre-seismic stage the elastic degradation is localised in a small area (one numerical element) and produces no geodetically significant signal. The dynamic weakening (15) and the proper elastic 3-D stress transfer calculated using the Green function (14) allow a failure in a hypocenter to extend into a region with possible complex geometry. The high healing rate in the post-seismic period increases the effective rigidity across the fault zone. The corresponding time scale, τ_h, is comparable to that reported by *Savage and Svarc* [1997] based on post-seismic deformation following the 1992 Landers earthquakes and by *Zhao et al.* [1997] based on inferred states of stress before and after the 1994 Northridge earthquake.

Ben-Zion and Rice [1993, 1995] and *Ben-Zion* [1996] simulated seismicity patterns along a strike-slip fault with fixed prescribed heterogeneities. Their models represent approximately geometric disorder of a fault zone by various types of disorder in strength properties. The simulations of the present work allow us to compare results from evolving complex structures with true geometric disorder to the simple planar approximations of

Ben-Zion and Rice. In our model, the ratio between the rates of loading and healing (τ_h/τ_L) provides a guideline for understanding the sensitivity of fault pattern evolution and earthquake statistics to τ_h that is evident in the simulations (Figures 8-14). When the system has long-term memory (τ_h/τ_L is high) it produces fast damage localisation during a time interval less than one earthquake cycle. This leads to the development of geometrically regular fault systems and frequency-size event statistics compatible with the characteristic earthquake distribution. In such cases, the event statistics are similar to those simulated by model realizations of *Ben-Zion and Rice* [1993, 1995] and *Ben-Zion* [1996] with relatively regular heterogeneities. Conversely, a system lacking short term memory (τ_h/τ_L is relatively low) develops highly disordered fault systems and produces power-law frequency-size statistics compatible with the Gutenberg-Richter distribution. In these cases, the event statistics are similar to those simulated by model realizations of Ben-Zion and Rice with highly disordered heterogeneities. The correlation between fault complexity and frequency-size statistics suggested by the present model and the previous simulations of *Ben-Zion and Rice* [1993, 1995] and *Ben-Zion* [1996] are in agreement with field and seismological observations of *Wesnousky* [1994] and *Stirling et al.* [1996].

A model with random intrinsic heterogeneity expressed by small amplitude variation in spatial distribution of the dynamic weakening τ_r and modified internal friction ξ_0, generates a power law frequency-size statistics with a b-value of 1.3. This value falls in the range of the observed b = 0.7-1.35 in regional and global earthquake catalogs [*Frohlich and Davis*, 1993].

For some ratio of time scales τ_h/τ_L, the results exhibit alternating overall switching of response, from a period with frequency-size statistics following characteristic distribution to a period with Gutenberg-Richter statistics and back (Figure 14). In the periods associated with the characteristic distribution the largest possible events in the system occur, while in the periods associated with the Gutenberg-Richter statistics there are only small and intermediate size earthquakes. *Ben-Zion et al.*, [1999b] discuss the similarity of these results to those found by *Dahmen et al.* [1998]. Long term switching of seismic activity between relatively active and relatively quiet time intervals has been indicated by disturbed sediments and surface

faulting in the Dead Sea transform, in a continuous record spanning 50 thousand years [*Marco et al.*, 1996]. Qualitatively similar alternating deformation phases have been documented in the eastern California shear zone [*Rockwell et al.*, 1999], the Great Basin Province in the western US [*Wallace*, 1987], the Altyn Tagh fault in China [*G. King*, pers. com., 1998], and other locations [*Ben-Zion et al.*, 1999b]. In the Dead Sea transform sites studied by *Marco et al.* [1996], each active period may exceed 10 thousand years and contain up to 15 events, 7-10 fold more than in the relatively quiet periods. A similar picture would emerge from Figure 14 for events with M>7.5. The first half of the record shows a cluster with 17 M>7.5 events whereas the second shows only 4. The scaling of this model to the Dead Sea Transform should account for an order of magnitude lower loading rate [*Joffe and Garfunkel*, 1987; *Ellenblum et al.*, 1998; *Pe'eri, Wdowinsky, Bechor*, 1999].

Appendix: Numerical scheme

The system of equation that should be solved numerically consists from equation of motion of the hybrid model and equations describing damage evolution and transient stress redistribution. Here we rewrite all these equation with brief comments on numerical approach to their solution. We start with equation of motion (13)

$$H \cdot \iint_S G_{kn} \frac{\partial}{\partial t} \frac{\partial \sigma_{nm}}{\partial x_m} ds + \frac{Hh}{\eta} \frac{\partial \sigma_{km}}{\partial x_m} = \frac{\partial u_k}{\partial t} - V_{plate}^{(k)} \qquad (A1)$$

which is solved by iterative procedure similar to "FLAC" [*Cundall and Board*, 1988]. For the known elastic strain and all material parameters from the previous time step an iterative procedure gives new velocities $\left(V_i = \frac{\partial u_i}{\partial t} \right)$ in the simulated area. The computational Lagrangian mesh consists of quadrilateral elements, which are subdivided into pairs of constant-strain triangles, with different diagonals. This double overlay scheme ensures symmetry of the solution by averaging results obtained on two meshes. Linear triangular element shape functions L_k (k=1,3) are defined as:

$$L_k = a_k + x \cdot b_k + y \cdot c_k \qquad (A2)$$

where a_k , b_k ,c_k are constants and (x, y) are grid coordinates. These shape functions are used to interpolate the nodal velocities $v_i^{(k)}$ within each triangle element:

$$v_i(x,y) = \sum_{k=1}^{3} v_i^{(k)} \cdot L_k \qquad (A$$

This formula enables the calculation of the strain rate tensor e_{ij} in each triangle. The stress tensor σ_{ij} is calculated using elastic deformation, ε_{ij}, from the previous time step according to non-linear stress-strain elastic relations [*Lyakhovsky et al.*, 1997b]. Being

partially differentiated respect to time coordinate, this equation gives the relation between $\partial\sigma_{ij}/\partial t$ and strain rate tensor e_{ij}:

$$\frac{\partial\sigma_{11}}{\partial t} = \lambda e_{11} - \gamma\frac{\varepsilon_{11}e_{11} + \varepsilon_{22}e_{22} + 2\varepsilon_{12}e_{12}}{\sqrt{I_2}} + (2\mu - \gamma\xi)e_{11} -$$

$$-\gamma\varepsilon_{11}\left[\frac{e_{11} + e_{22}}{\sqrt{I_2}} - \xi\frac{\varepsilon_{11}e_{11} + \varepsilon_{22}e_{22} + 2\varepsilon_{12}e_{12}}{I_2}\right] +$$

$$+\frac{d\lambda}{dt}I_1 - \frac{d\gamma}{dt}\sqrt{I_2} + \left(2\frac{d\mu}{dt} - \frac{d\gamma}{dt}\xi\right)\varepsilon_{11}$$

(A4)

$$\frac{\partial\sigma_{22}}{\partial t} = \lambda e_{22} - \gamma\frac{\varepsilon_{11}e_{11} + \varepsilon_{22}e_{22} + 2\varepsilon_{12}e_{12}}{\sqrt{I_2}} + (2\mu - \gamma\xi)e_{22} -$$

$$-\gamma\varepsilon_{22}\left[\frac{e_{11} + e_{22}}{\sqrt{I_2}} - \xi\frac{\varepsilon_{11}e_{11} + \varepsilon_{22}e_{22} + 2\varepsilon_{12}e_{12}}{I_2}\right] +$$

$$+\frac{d\lambda}{dt}I_1 - \frac{d\gamma}{dt}\sqrt{I_2} + \left(2\frac{d\mu}{dt} - \frac{d\gamma}{dt}\xi\right)\varepsilon_{22}$$

$$\frac{\partial\sigma_{12}}{\partial t} = (2\mu - \gamma\xi)e_{12} - \gamma\varepsilon_{12}\left[\frac{e_{11} + e_{22}}{\sqrt{I_2}} - \xi\frac{\varepsilon_{11}e_{11} + \varepsilon_{22}e_{22} + 2\varepsilon_{12}e_{12}}{I_2}\right] + \left(2\frac{d\mu}{dt} - \frac{d\gamma}{dt}\xi\right)\varepsilon_{12}$$

When stresses σ_{ij} and their temporal derivation $\partial\sigma_{ij}/\partial t$ are known, the vector (F_i) on the left side of the equation (a1) at each node is used for calculation of new velocities by simple iterative procedure:

$$v_i^+ = v_i^- + \chi\left(F_i + V_{plate} - v_i^-\right) \qquad (A$$

The iteration parameter χ provide a convergence of the procedure, which is repeated until the maximum difference between previous v_i^- and next v_i^+ values of velocities become negligibly small.

Calculated velocity distribution is used for the Lagrangian transport equation for node coordinates

$$x_i^+ = x_i^- + v_i \cdot dt, \qquad ($$

and new total strain

$$\varepsilon_{ij}^+ = \varepsilon_{ij}^- + \frac{1}{2}\left(\frac{\partial v_i}{\partial x_j} + \frac{\partial v_j}{\partial x_i}\right) \cdot dt \qquad (A7$$

New z-component of elastic strain is defined according to the average lithostatic pressure (σ_{zz}= -ρ g H/2):

$$\varepsilon_{zz} = -\frac{1}{\lambda^e + 2\mu^e}\left[\lambda^e\left(\varepsilon_{xx} + \varepsilon_{yy}\right) + \rho g \frac{H}{2}\right] \qquad (A8)$$

New thickness of the upper crust is calculated using continuity equation (div (v_i) = 0) and local isostasy assumption:

$$H^+ = H^- \cdot \left[1 - \left(\frac{\partial v_x}{\partial x} + \frac{\partial v_y}{\partial y}\right) \cdot dt\right] \qquad (A9)$$

New damage distribution is calculated using evolution equation:

$$\alpha^{+} = \alpha^{-} + \left[C_d \cdot I_2 \cdot (\xi - \xi_0)\right] \cdot dt \text{, for degradation } (\xi > \xi_0)$$

$$\alpha^{+} = \alpha^{-} + \left[\alpha \cdot C_1 \cdot \exp\left(\frac{\alpha}{C_2}\right) \cdot I_2 \cdot (\xi - \xi_0)\right] \cdot dt \text{, for healing } (\xi < \xi_0)$$

The time step, dt, used for all these numerical procedures are selected after two conditions: 1) Damage change in each time step does not exceed some constant value ($\Delta\alpha_{max}$) selected by comparing a series of similar runs

$$dt_{damage} = \frac{(\Delta\alpha)_{max}}{\left(\frac{d\alpha}{dt}\right)_{max}} \qquad (A$$

2) Numerical stability of the parabolic equation (a1) based on the Fourier stability analysis require that the time step Δt is less then half of the relaxation time of the shortest wave length, related to the grid size Δx [*Ames*, 1977]. The upper boundary for the time step used in the simulations is equal to one third of the characteristic time of the attenuation of the wave with length equal to Δx:

$$\Delta t_{max} = \frac{1}{3} \cdot \frac{\Delta x^2}{h H \mu / \eta} < \frac{1}{3} \cdot \frac{\Delta x^2 + H\mu G_{yy}\left(\frac{2\pi}{\Delta x}\right)}{h H \mu / \eta} \qquad (A12)$$

At some stage of evolution the level of damage in one or several elements achieve the critical level, corrected after the dynamic weakening (15). These elements can not further keep stress, which should be dropped. The immediate change of the stress $\Delta\sigma_{ij}$ is equivalent to distributed force along the element boundary, S, with vector n_k normal to it:

$$F_j = \Delta\sigma_{jk} n_k \qquad (A$$

and the co-seismic elastic displacements are calculated using the Green function (14)

$$u_k^{(e)} = \iint_S G_{kj} \cdot F_j ds \qquad (A1$$

The elements involved in the failure process accumulate the plastic strain components that are recorded together with the values of the stress drop for the further calculation of the earthquake moment and potency.

References:

Agnon, A., V.Lyakhovsky, and Y.Ben-Zion, A continuum approach to rock friction. 1999 (in preparation).

Ames, W.F., Numerical methods for partial differential equations. Academic Press, 365 p., 1977.

Amelung, F. and G. King, Earthquake scaling laws for creeping and non-creeping faults, *Geophys. Res. Lett.*, 24, 507-510, 1997.

Andrews, D. J., Coupling of energy between tectonic processes and Earthquakes, *J. Geophys. Res.*, 83, 2259-2264, 1978.

Andrews, D. J., Mechanics of fault junctions, *J. Geophys. Res.*, 94, 9389-9397, 1989.

Andrews, D.J. and Y.Ben-Zion, Wrinkle-like Slip Pulse on a Fault Between Different Materials, *J. Geophys. Res.*, 102, 553-571, 1997.

Anooshehpoor A. and J. N. Brune, Wrinkle-like Weertman pulse at the interface between two blocks of foam rubber with different velocities, *Geophys. Res. Lett.*, 26, 2025-2058, 1999.

Ben-Menahem A. and S.J.Singh, Seismic waves and sources, Springer-Verlag, New York, 1981.

Ben-Zion, Y., The response of two jointed quarter spaces to SH line sources located at the material discontinuity interface, *Geophys. J. Int.*, 98, 213-222, 1989.

Ben-Zion, Y., Stress, slip and earthquakes in models of complex single-fault systems incorporating brittle and creep deformations, *J. Geophys. Res.*, 101, 5677-5706, 1996.

Ben-Zion, Y., and D.J.Andrews, Properties and implications of dynamic rupture along a material interface, *Bull. Seismol. Soc. Amer.*, 88, 1085-1094, 1998.

Ben-Zion, Y. and J. R. Rice, Earthquake failure sequences along a cellular fault zone in a 3D elastic solid containing asperity and nonasperity regions, *J. Geophys. Res.*, 98, 14109-14131, 1993.

Ben-Zion, Y. and J. R. Rice. Slip patterns and earthquake populations along different classes of faults in elastic solids, *J. Geophys. Res.*, 100, 12,959-12,983, 1995.

Ben-Zion, Y. and J. R. Rice, Dynamic simulations of slip on a smooth fault in an elastic solid, *J. Geophys. Res.*, 102, 17771-17784, 1997.

Ben-Zion, Y., J. R. Rice and R. Dmowska, Interaction of the San Andreas fault creeping segment with adjacent great rupture zones and earthquake recurrence at Parkfield, *J. Geophys. Res.*, 98, 2135-2144, 1993.

Ben-Zion, Y. C. Sammis and T. Henyey, Perspectives on the Field of Physics of Earthquakes, *Seism. Res. Lett.*, 70, 428-431, 1999a.

Ben-Zion, Y., K. Dahmen, V. Lyakhovsky, D. Ertas and A. Agnon, Self-Driven Mode Switching of Earthquake Activity on a Fault System, *Earth Planet. Sci. Lett.*, 172, 11-21, 1999b.

Brune J.N., T.L.Henyey and R.F.Roy, Heat flow, stress and rate of slip along the San Andreas Fault, California, *J. Geophys. Res.*, 74, 3821-3827, 1969.

Brune, J.N., S.Brown and P.A.Johnson, Rupture mechanism and interface separation in foam rubber model of earthquakes: a possible solution to the heat flow paradox and the paradox of large overthrusts, *Tectonophysics*, 218, 59-67, 1993.

Chinnery, M.A., The deformation of the ground around surface faults. *Bull. Sesmol. Soc. Am.*, 51, 355-372, 1961.

Cundall, P.A. and M. Board, A microcomputer program for modeling large-strain plasticity problems. In: C.Swoboda (Ed.), Numerical methods in geomechanics, Proc. 6th Int. Conf. Numerical Methods in Geomechanics, Innsbruck. Balkhema, Rotterdam, pp. 2101-2108, 1988.

Dahmen, K., D. Ertas and Y. Ben-Zion, Gutenberg Richter and Characteristic Earthquake behavior in Simple Mean-Field Models of Heterogeneous Faults, *Phys. Rev. E*, 58, 1494-1501, 1998.

Dieterich, J. H., Earthquake nucleation on faults with rate- and state-dependent strength, *Tectonophysics*, 211, 115-134, 1992.

Ellenblum, R., S. Marco, A. Agnon, T. Rockwell and A. Boas, A Crusader castle torn apart by the 1202 Earthquake, *Geology*, 26, 303-306, 1998.

Elsasser, W.M., Convection and stress propagation in the upper mantle, in *The Application of Modern Physics to the Earth and Planetary Interiors*, edited by S.K. Runcorn, pp. 223-246, Wiley-Interscience, New York, 1969.

England, P.C. and D.P. McKenzie, A thin viscous sheet model for continental deformation. *Geophys. J. R. Astron. Soc.* 70, 295-321, 1982.

Frohlich, C. and S. D. Davis, Teleseismic *b* values; or, much ado about 1.0, *J. Geophys. Res.*, 98, 631-644, 1993.

Fuis, G. S., and W. D. Mooney, Lithospheris structure and tectonics from seismic-refraction and other data, in *The San Andreas Fault System, California, edited by R. E. Wallace, U.S. Geol. Surv. Prof. Pap.*, 1515, 207-238, 1990.

Gabrielov, A. and W. I. Newman, Seismicity modeling and earthquake prediction: a review, in Nonlinear Dynamics and Predictability of Geophysical Phenomena, Geophys. Mon.. 83, IUGG 18, 7-13, 1994.

Hanks, T.C. and H.Kanamori, A moment magnitude scale, *J. Geophys. Res.*, 84, 2348-2350, 1979.

Harris, R. A. and R. W. Simpson, In the shadow of 1857- the effect of the great Ft. Tejon earthquake on subsequent earthquakes in southern California, *Geophys. Res. Letters*, 23, 229-232, 1996.

Heaton, T.H., Evidence for and implications of the self-healing pulses of slip in earthquake rupture, *Phys. Earth Planet. Int.*, 64, 1-20, 1990.

Heaton H.T. and R.E.Heaton, Static deformation from point forces and force couples located in welded elastic Poissonian half-spaces: implications for seismic moment tensors, *Bull. Seismol. Soc. Amer* 79, 813-841, 1989.

Heimpel M. and P. Olson, A seismodynamical model of lithosphere deformation: Development of continental and oceanic rift networks. *J. Geophys. Res.* 101, 16155-16176, 1996.

Joffe, S. and Z. Garfunkel, Plate kinematics of the circum Red Sea – a re-evaluation, *Tectonophysics*, 141, 5-22, 1987.

Kanamori H. and D.L.Anderson, Theoretical basis of some empirical relations in seismology. *Bull. Seismol. Soc. Am.* 65, 1073-1095, 1975.

Kasahara, K., Earthquake mechanics. Cambridge Univ. Press. pp. 248, 1981

King, G., The accommodation of large strains in the upper lithosphere of the earth and other solids by self-similar fault systems: the geometrical origin of b-value, *Pure Appl. Geophys.*, 121, 761-814, 1983.

Lachenbruch, A. H., and J. H. Sass, Thermo mechanical aspects of the San Andreas, Proceedings, Conference on the Tectonic Problems of the San Andreas Fault System, edited by R. L. Kovach and A. Nur, Stanford Univ. Publ. Geol. Sci., 13, 192-205, 1973.

Landau L.D., and E.M. Lifshitz, Theory elasticity, 2nd edn, Pergamon, Oxford, 1970

Lehner, F. K., V. C. Li, and J. R. Rice, Stress diffusion along rupturing plate boundaries, *J. Geophys. Res.*, 86, 6155-6169, 1981.

Li, V.C. and J.R. Rice, Crustal deformation in great California earthquake cycles, *J. Geophys. Res.*, 92, 11,533-11,551, 1987.

Lisowski, M., J.C.Savage, and W.H.Prescott, The velocity field along the San Andreas fault in central and southern California, *J. Geophys. Res.*, 96, 8369-8389, 1991.

Lyakhovsky, V., Y. Ben-Zion, and A. Agnon, Distributed damage, faulting, and friction, *J. Geophys. Res.*, 102, 27,635-27,649, 1997a.

Lyakhovsky, V., Z.Reches, R.Weinberger and T.E.Scott, Non-linear elastic behavior of damaged rocks, *Geophys. J. Int.*, 130, 157-166, 1997b.

Madariaga, R., 1979. On the relation between seismic moment and stress drop in the presence of stress and strength heterogeneity. *J. Geophys. Res.*, 84:2243-2250

Marco, S., M. Stein, A. Agnon, and H. Ron, Long-term earthquake clustering: a 50,000-year paleoseismic record in the Dead Sea graben, *J. Geoph. Res.*, 101, 6179-6191, 1996.

Meisner, R., and J. Strehlau, Limits of stress in continental crusts and thier relation to the depth-frequency distribution of shallow earthquakes, *Tectonics*, 1, 79-83, 1982.

Mooney, W. D., G. Laske, and T. G. Masters, CRUST 5.1: A global crustal model at 5^0 x 5^0, *J. Geophys. Res.*, 103, 727-747, 1998.

Mora, P. and D.Place, Simulation of the frictional stick-slip insability, *Pure Appl. Geophys.* 143, 61-87, 1994.

Ohnaka, M., Non-uniformity of the constitutive law parameters for shear rupture and quasi-static nucleation to dynamic rupture: A physical model of earthquake generation processes, *Proc. Natl. Acad. Sci. U.S.A.*, **93**, 3795-3802, 1996.

Okubo, P. G., Dynamic rupture modeling with laboratory-derived constitutive relations, *J. Geophys. Res.*, 94, 12,321-12,335, 1989.

Pe'eri, S., S. Wdowinsky, A. Stibelman, N. Bechor and Y. Bock, Current deformation across the Dead Sea fault as observed from 18 month of continuous GPS monitoring, In: proc of Annual meeting, Israel Geol. Soc., 1999.

Reches, Z., G. Schubert, and C. Anderson, Modeling of periodic great earthquakes on the San Andreas fault: Effects of nonlinear crustal rheology, *J. Geophys. Res.*, 99, 21,983-22,000, 1994.

Rice, J. R., 1980. The mechanics of Earthquake rupture. In: Physics of the Earth's interior. North-Holland. pp. 555-649.

Rice, J. R., Spatio-temporal complexity of slip on a fault, *J. Geophys. Res.*, **98**, 9885-9907, 1993.

Robinson, R. and R. Benites, Synthetic seismicity models of multiple interacting faults, *J. Geophys. Res.*, 100, 18229-18238, 1995.

Rockwell, T. K. S. Lindvall, M. Herzberg, D. Murbach, T. Dawson, and G.Berger, Paleoseismology of the Johnson Valley, Kickcapoo and Homestead Valley faults of the Eastern California Shear Zone, *Bull. Seismol. Soc. Amer.*, in review (1999).

Savage, J.C., Dislocations in seismology, in: *Dislocations in Solids*, vol. 3, edited by F.R.N. Nabarro, pp. 251-339, North-Holland, New York, 1980.

Savage,J.C., Equivalent strike-slip earthquake cycles in half-space and lithosphere-asthenosphere Earth models, *J. Geophys. Res.*, 95, 4873-4879, 1990.

Savage, J.C. and J.L.Svarc, Post seismic deformation associated with the 1992 M_W=7.3 Landers earthquake, southern California, *J.Geophys. Res.*, 102, 7565-7577, 1997.

Scholz, C. H., N. H. Dawers, J.-Z. Yu, M. H. Anders and P. A. Cowie, Fault growth and fault scaling laws: Preliminary results, *J. Geophys. Res.*, 98, 21951-21961, 1993.

Sibson, R. H., Fault zone models, heat flow, and the depth distribution of earthquakes in the continental crust of the United States, *Bull. Sesmol. Soc. Am.*, 72, 151-163, 1982.

Simpson, R. W., and P. A. Reasenberg, Earthquake-induced static stress changes on central California faults, in the Loma Prieta, California earthquake of October 17, 1989-tectonic processes and models, R. W. Simpson (Ed.), U. S. Geological Survey Prof. Paper 1550-F, 1994.

Shibazaki, B. and M. Matsu'ura, Spontaneous processes for nucleation, dynamic propagation, and stop of earthquake rupture, *Geophys. Res. Lett.*, **19**, 1189-1192, 1992.

Sornette, D. P. Miltenberger and C. Vanneste, Statistical physics of fault patterns self-organized by repeated earthquakes, *Pure Appl. Geophys.*, 142, 491-527, 1994.

Stein, R. S., A. A. Barka and J. H. Dieterich, Progressive failure on the North Anatolian fault since 1939 by earthquake stress triggering, *Geophys. J. Int.*, 128, 594-604, 1997.

Stein, R. S., G. King and J. Lin, Stress triggering of the 1994 M-6.7 Northridge, California, earthquake by its predecessors, *Science*, 265, 1432-1435, 1994.

Stirling, M.W., S.G. Wesnousky and K. Shimazaki, Fault trace complexity, cumulative slip , and the shape of the magnitude-frequency distribution for strike-slip faults: a global survey, *Geophys. J. Int.*, 124, 833-868, 1996.

Thatcher, W., Nonlinear strain build-up and earthquake cycle on the San Andreas fault, *J. Geophys. Res.*, 88, 5893-5902, 1983.

Wallace, R. E., Grouping and migration of surface faulting and variations in slip rates on faults in the great basin province, *Bull. Seismol. Soc. Amer.*, 77, 868-876, 1987.

Ward, S., A synthetic seismicity model for southern California: cycles, probabilities, hazard, *J. Geophys. Res.*, 101, 22393-22418, 1996.

Wesnousky, S.G., The Gutenberg-Richter or characteristic earthquake distribution, which is it? *Bull. Seismol. Soc. Amer.*, 84, 1940-1959, 1994.

Wdowinski, S., and R.J. O'Connell, On the choice of boundary conditions in continuum models of continental deformation, *Geophys. Res. Lett.*, 17, 2413-2416, 1990.

Zhao, D., H.Kanamori and D.Wiens, State of stress before and after the 1994 Northridge earthquake, *Geophys. Res. Lett.*, 24, 519-522, 1997.

Zoback, M. and G.C. Beroza, Evidence for near-frictionless faulting in the 1989 (M-6.9) Loma-Prieta, California, earthquake and its aftershocks, *Geology*, 21, 181-185, 1993.

Figure caption

Fig. 1 Brittle upper crust (H=15 km) coupled to a visco-elastic lower crust (h=20 km) driven by mantle movement (V_{plate}).

Fig. 2 Relaxation time of the original Elsasser, Generalized Elsasser and Hybrid models for viscosity of the lower crust η=5 10^{19} Pa s.

Fig. 3 Fault-parallel velocity at 10 and 20 km of the fault as a function of time for the Generalized Elsasser and the Hybrid models

Fig. 4 Velocity profiles 100 years after the large earthquake simulated for the model with relaxation times τ_m = 5, 12.5, and 25 years. Gray line represents the best fit of geodetic data with dislocation model after *Savage* [1990].

Fig. 5 Strain diagonality (ξ) and damage (α) evolution during earthquake cycle for a single fault model. Damage rate constants: C_d=0.1 s^{-1}; C_1=10^{-10} s^{-1}; C_2=0.05.

Fig. 6 Correlation between earthquake magnitudes calculated using seismic moment and potency.

Fig. 7 Material recovering (damage versus time) under constant lithostatic pressure for different healing rate constants.

Fig. 8 Cumulated strain (a) and damage distribution (b) for the model with slow healing.

Fig. 9 Statistics of seismic events, logarithm numbers versus magnitude, for slow damage healing (long material memory) and different τ_d.

Fig. 10 Statistics of seismic events, logarithm numbers versus magnitude, for medium damage healing and different damage rate constants C_d.

Fig. 11 Cumulated strain (a) and damage distribution (b) for the model with fast healing.

Fig. 12 Statistics of seismic events, logarithm numbers versus magnitude, for fast damage healing.

Fig. 13 Statistics of seismic events, logarithm numbers versus magnitude, for fast damage healing and spatial variations of material strength.

Fig. 14 Record of seismic events demonstrates switching between activating periods and low activity period. Inserts A, B, C, show the distribution of seismic events induced by the three strongest events.

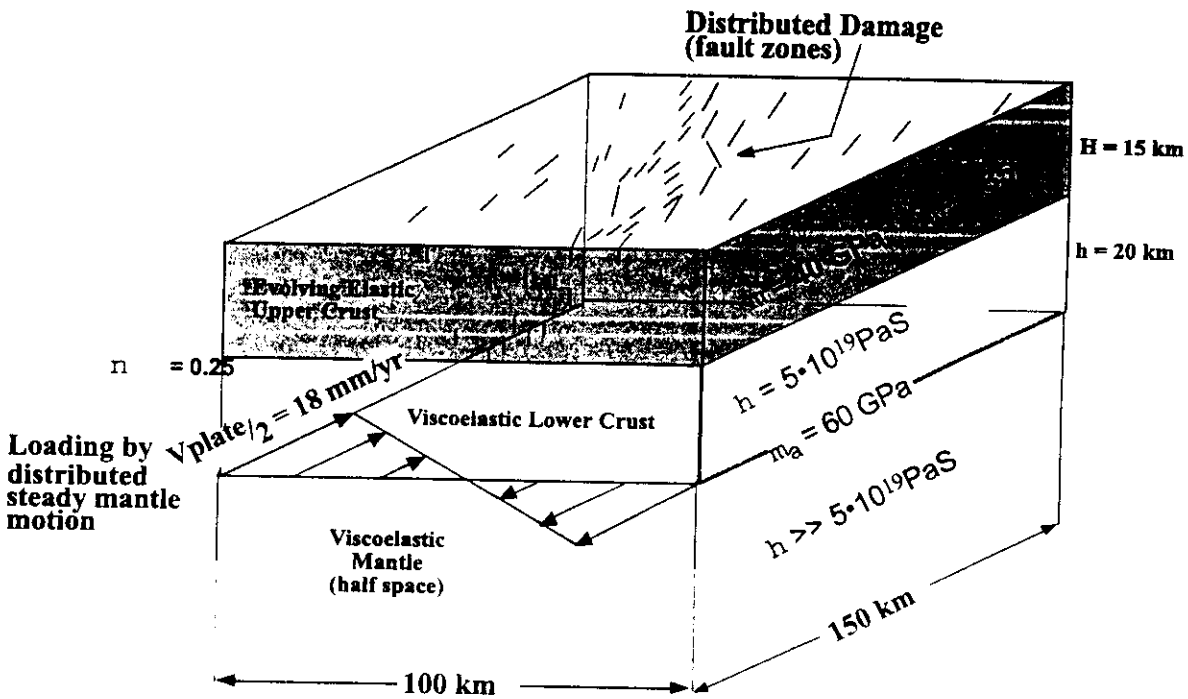
Distributed Damage
(fault zones)
H = 15 km
h = 20 km
Evolving Elastic
Upper Crust
n = 0.25
Viscoelastic Lower Crust
h = 5•10^19PaS
μa = 60 GPa
h >> 5•10^19PaS
Loading by
distributed
steady mantle
motion
Viscoelastic
Mantle
(half space)
100 km
150 km

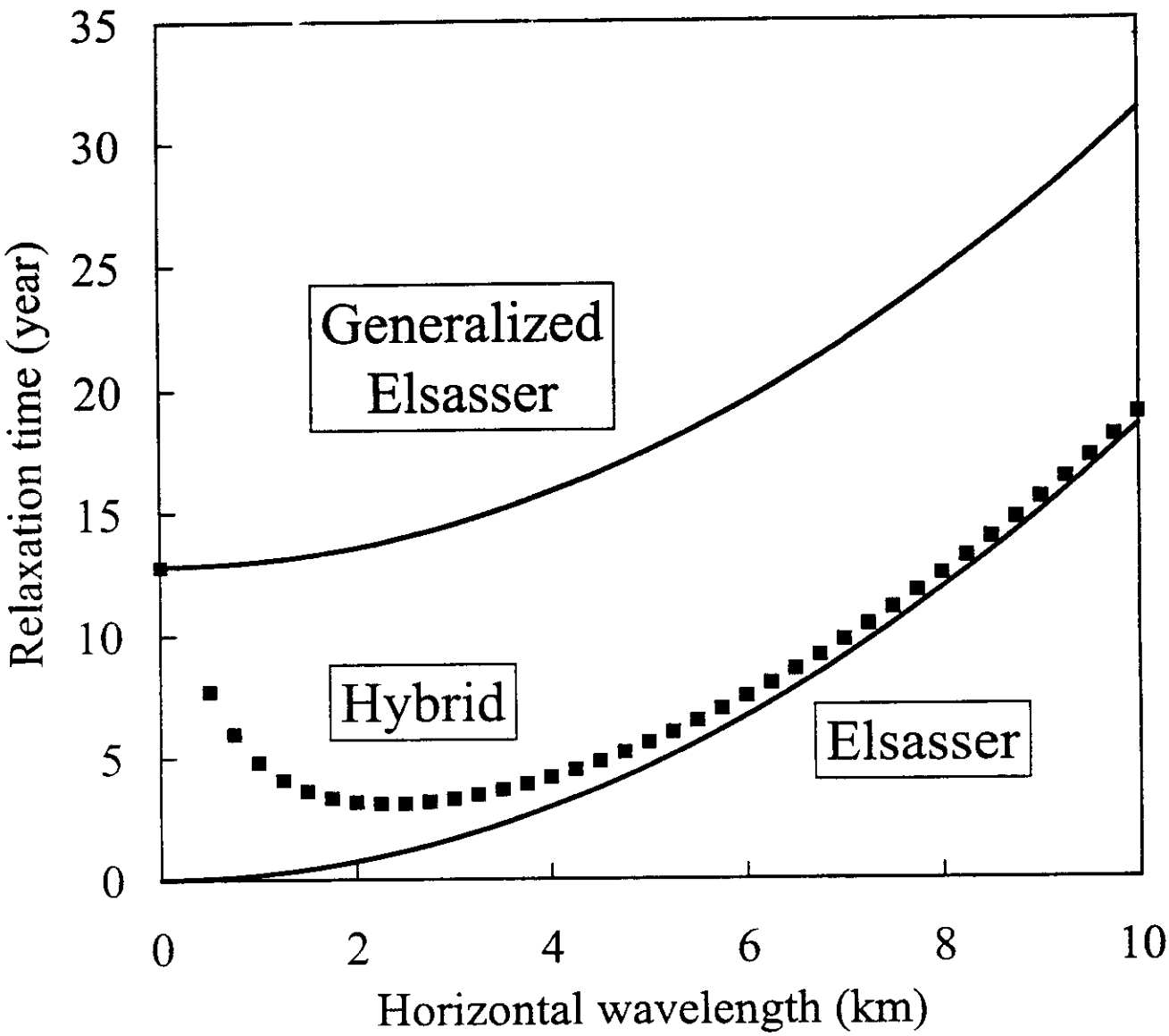
35
30
25
20
15
10
5
0
Relaxation time (year)
Generalized
Elsasser
Hybrid
Elsasser
0
2
4
6
8
10
Horizontal wavelength (km)

Figure 2

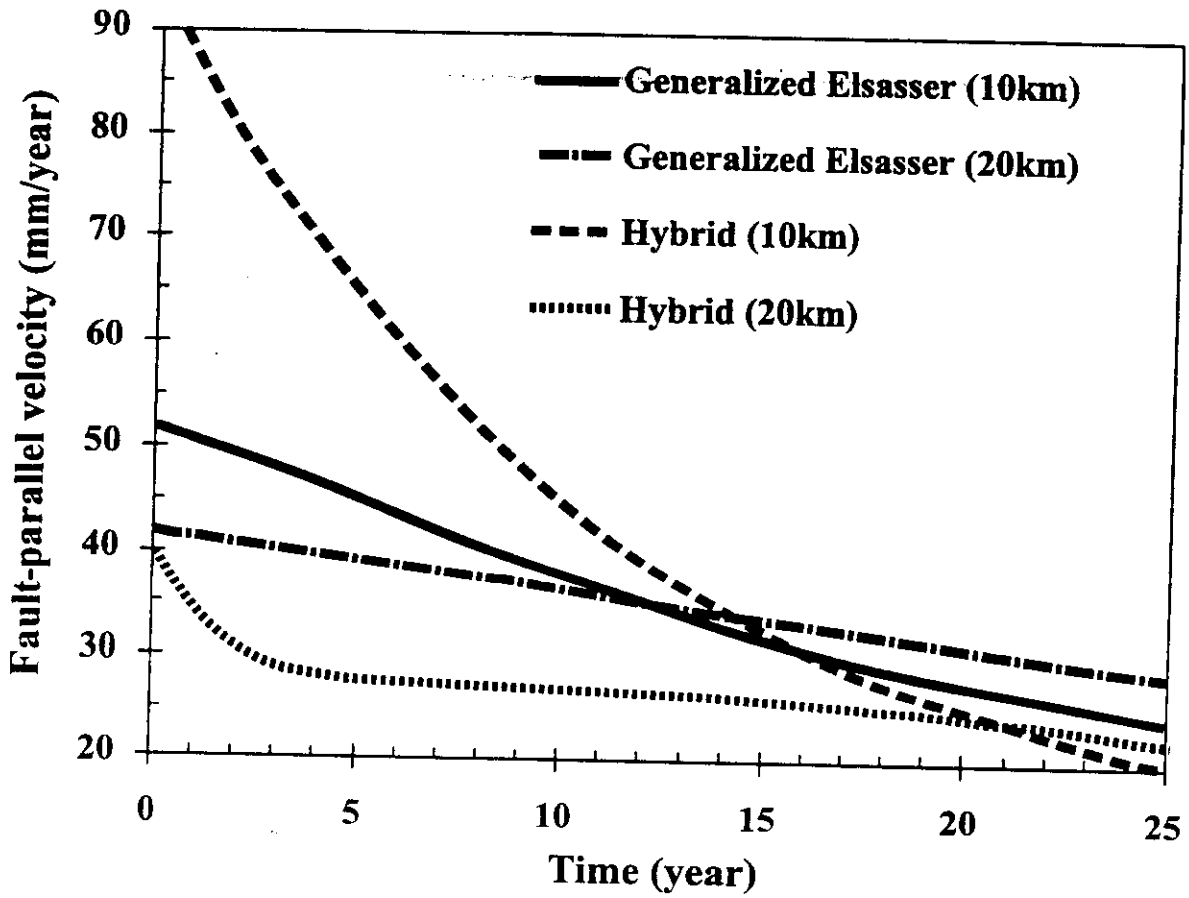
Generalized Elsasser (10km)
Generalized Elsasser (20km)
Hybrid (10km)
Hybrid (20km)
Fault-parallel velocity (mm/year)
90
80
70
60
50
40
30
20
0
5
10
15
20
25
Time (year)

Fig. 3

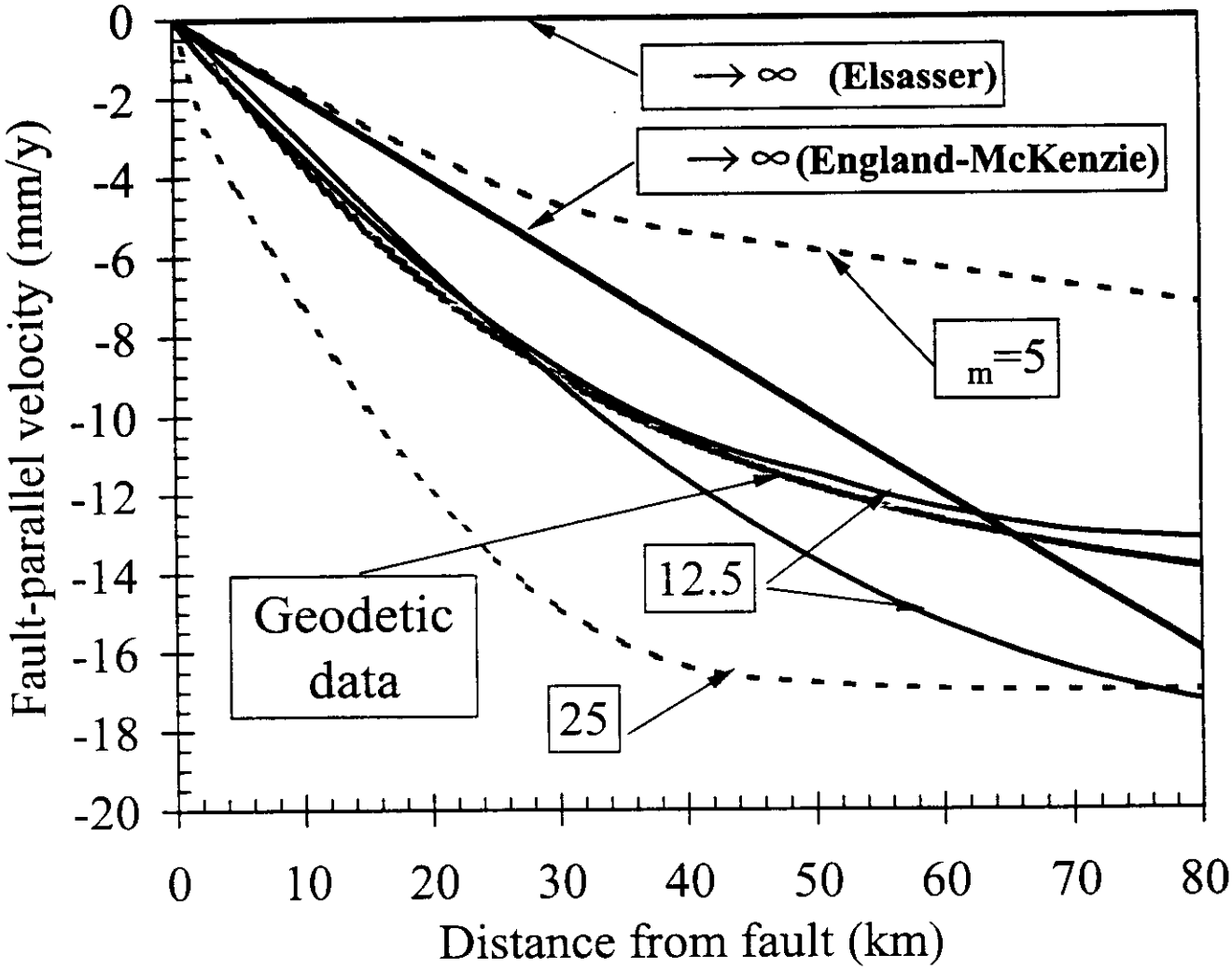
0
-2
-4
-6
-8
-10
-12
-14
-16
-18
-20
Fault-parallel velocity (mm/y)
0
10
20
30
40
50
60
70
80
Distance from fault (km)
→ ∞ (Elsasser)
→ ∞ (England-McKenzie)
m=5
12.5
25
Geodetic data

Fig. 4

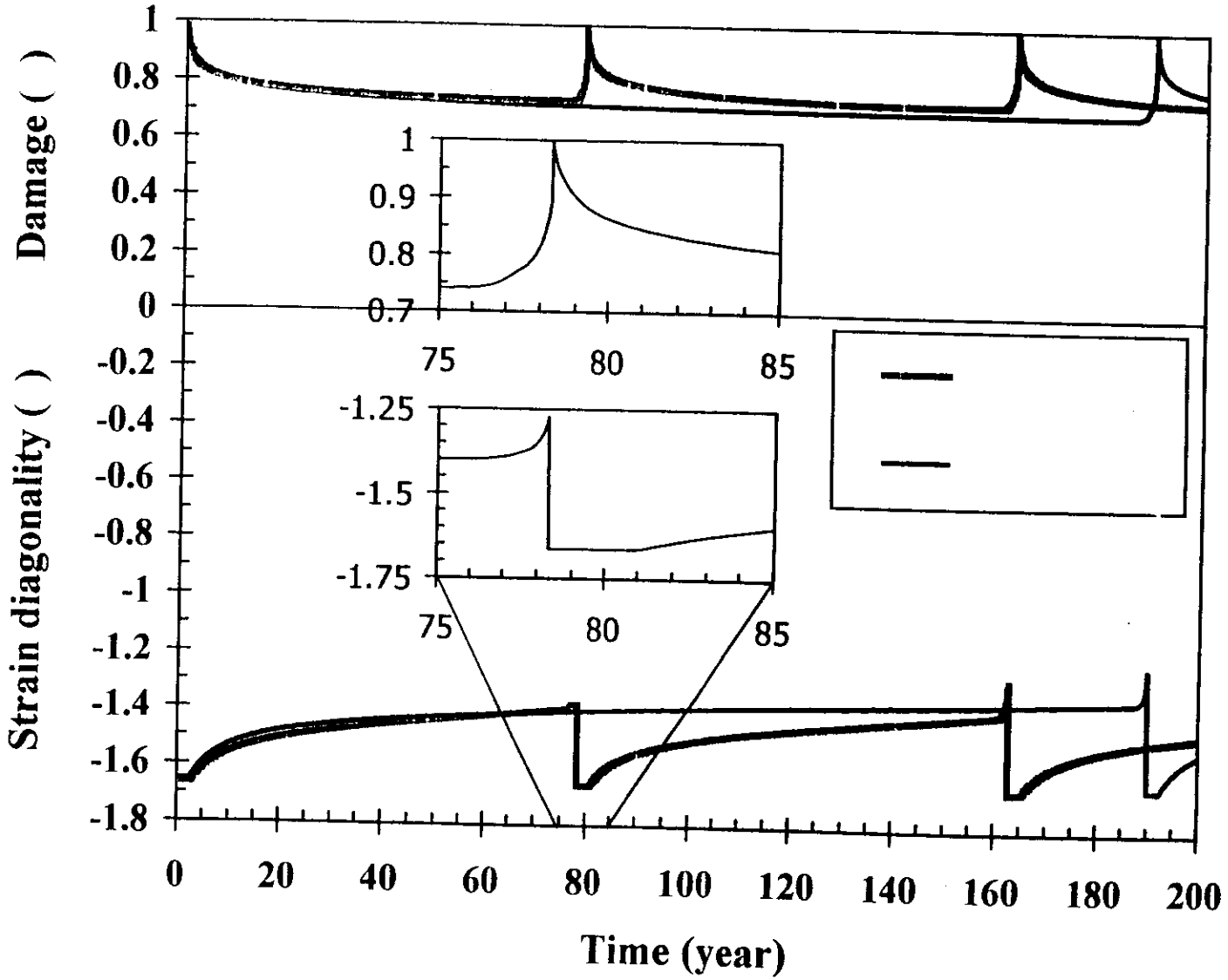
Damage ( )
Strain diagonality ( )
Time (year)
1
0.8
0.6
0.4
0.2
0
-0.2
-0.4
-0.6
-0.8
-1
-1.2
-1.4
-1.6
-1.8
0
20
40
60
80
100
120
140
160
180
200
1
0.9
0.8
0.7
75
80
85
-1.25
-1.5
-1.75
75
80
85

Fig. 5

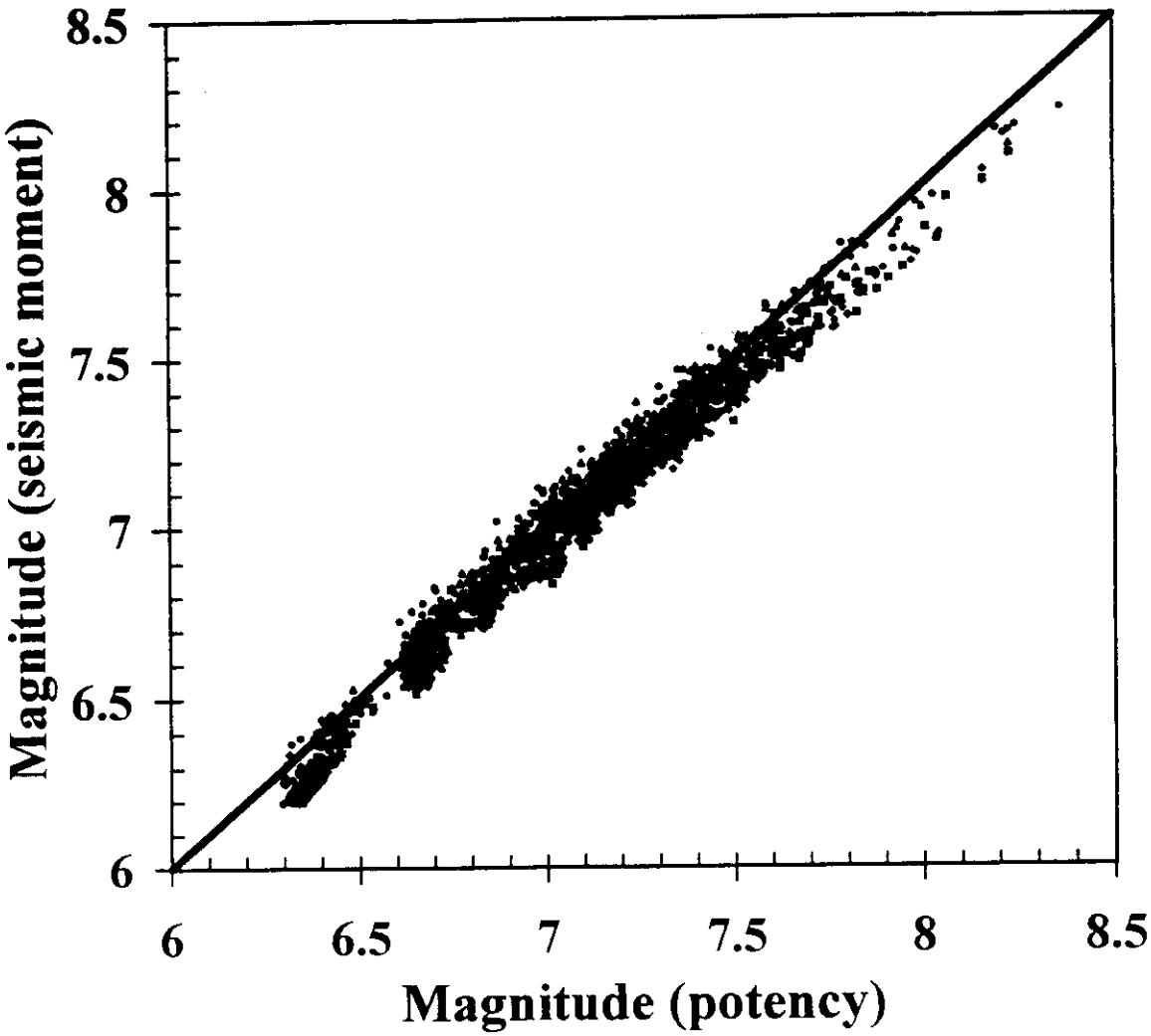
8.5
8
7.5
7
6.5
6
Magnitude (seismic moment)
6
6.5
7
7.5
8
8.5
Magnitude (potency)

Fig. 6

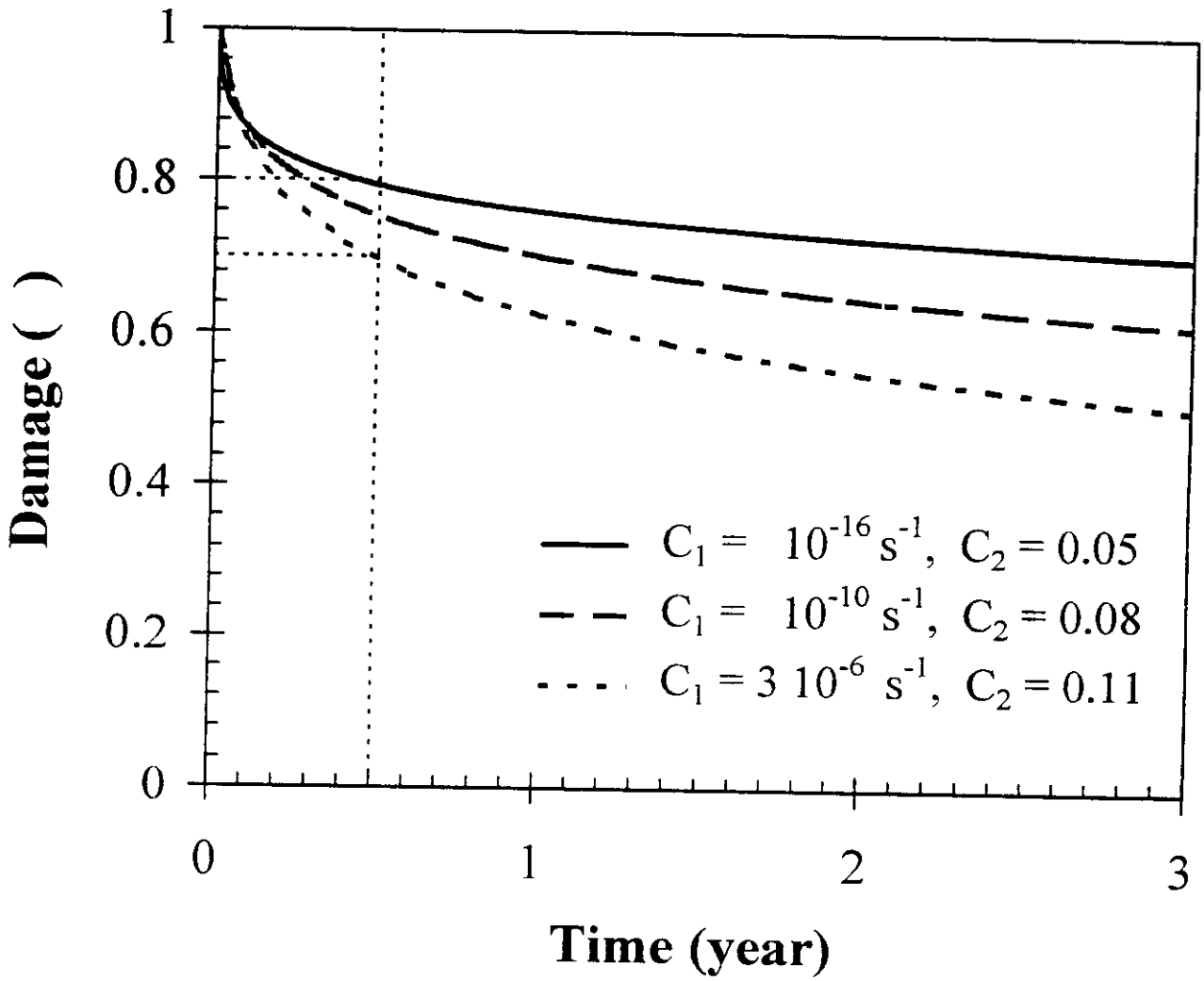
1
0.8
0.6
0.4
0.2
0
Damage ( )
0
1
2
3
Time (year)
C1 = 10-16 s-1, C2 = 0.05
C1 = 10-10 s-1, C2 = 0.08
C1 = 3 10-6 s-1, C2 = 0.11

Fig. 7

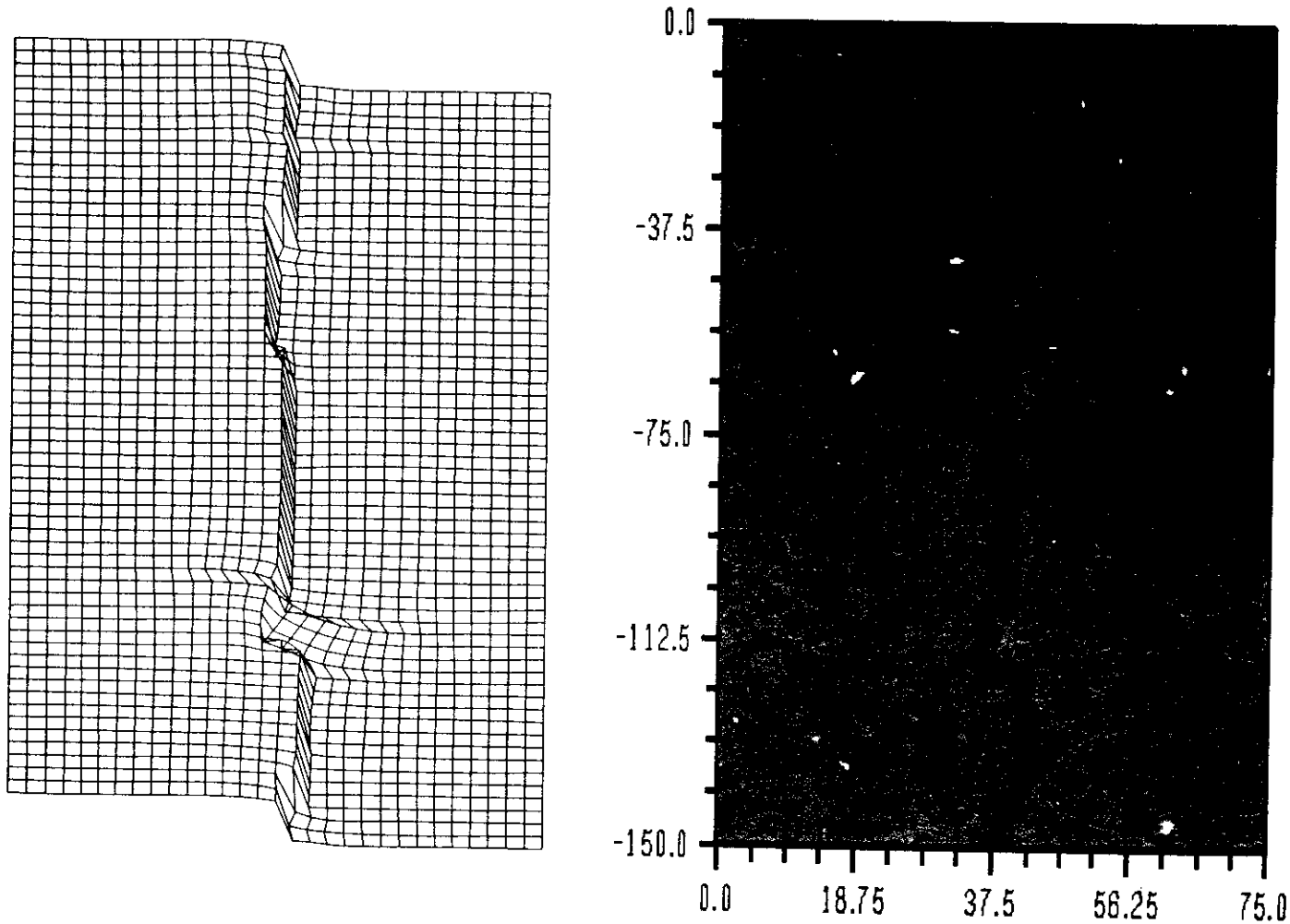
0.0
-37.5
-75.0
-112.5
-150.0
0.0
18.75
37.5
56.25
75.0

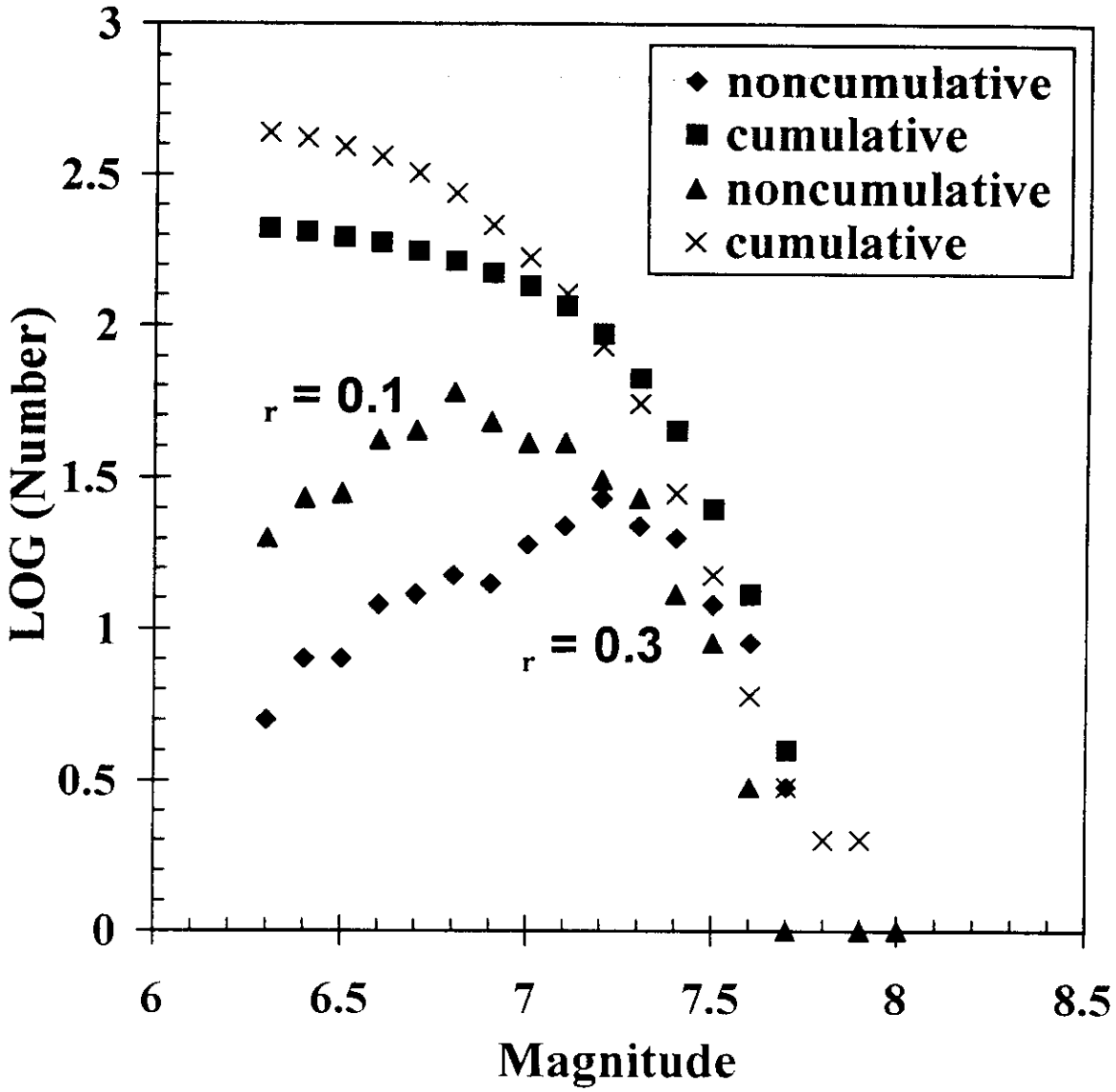
noncumulative
cumulative
noncumulative
cumulative
r = 0.1
r = 0.3
LOG (Number)
Magnitude
3
2.5
2
1.5
1
0.5
0
6
6.5
7
7.5
8
8.5

Fig. 9

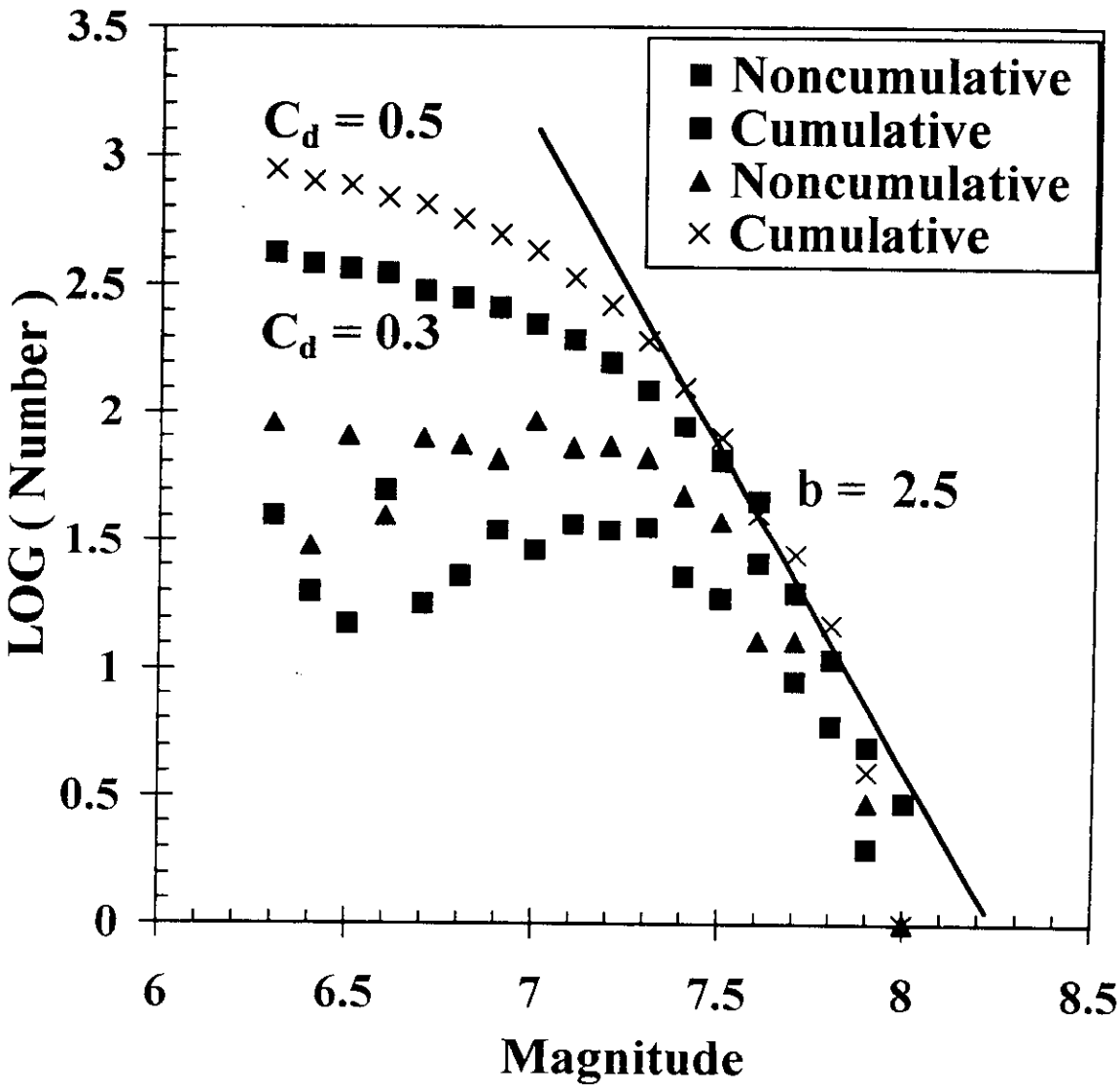
3.5
3
2.5
2
1.5
1
0.5
0
LOG (Number)
6
6.5
7
7.5
8
8.5
Magnitude
Noncumulative
Cumulative
Noncumulative
Cumulative
$C_d = 0.5$
$C_d = 0.3$
b = 2.5

Fig. 10

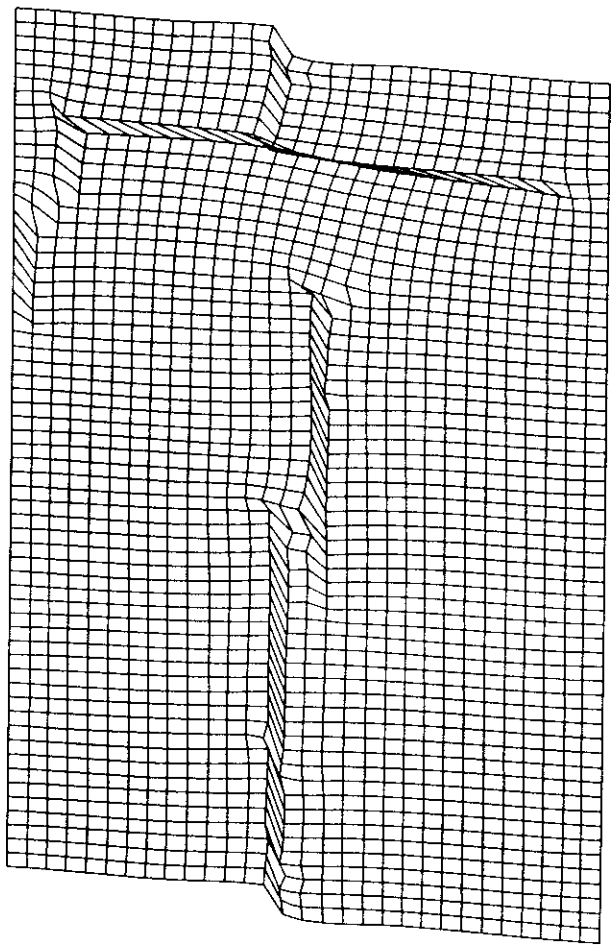

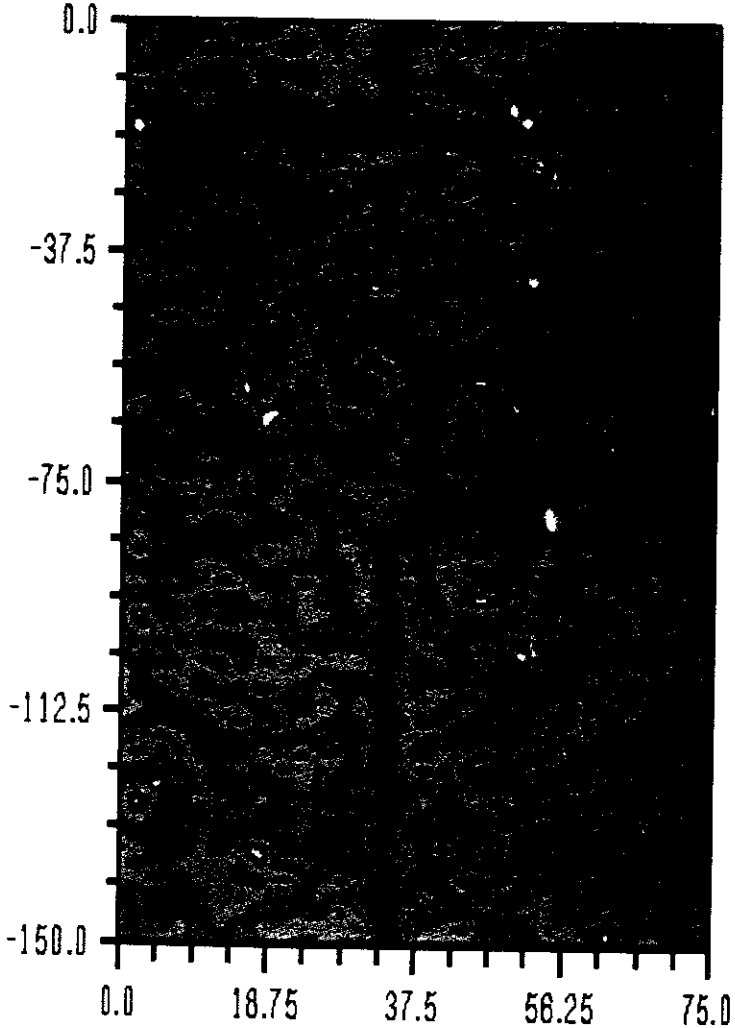
0.0
-37.5
-75.0
-112.5
-150.0
0.0
18.75
37.5
56.25
75.0

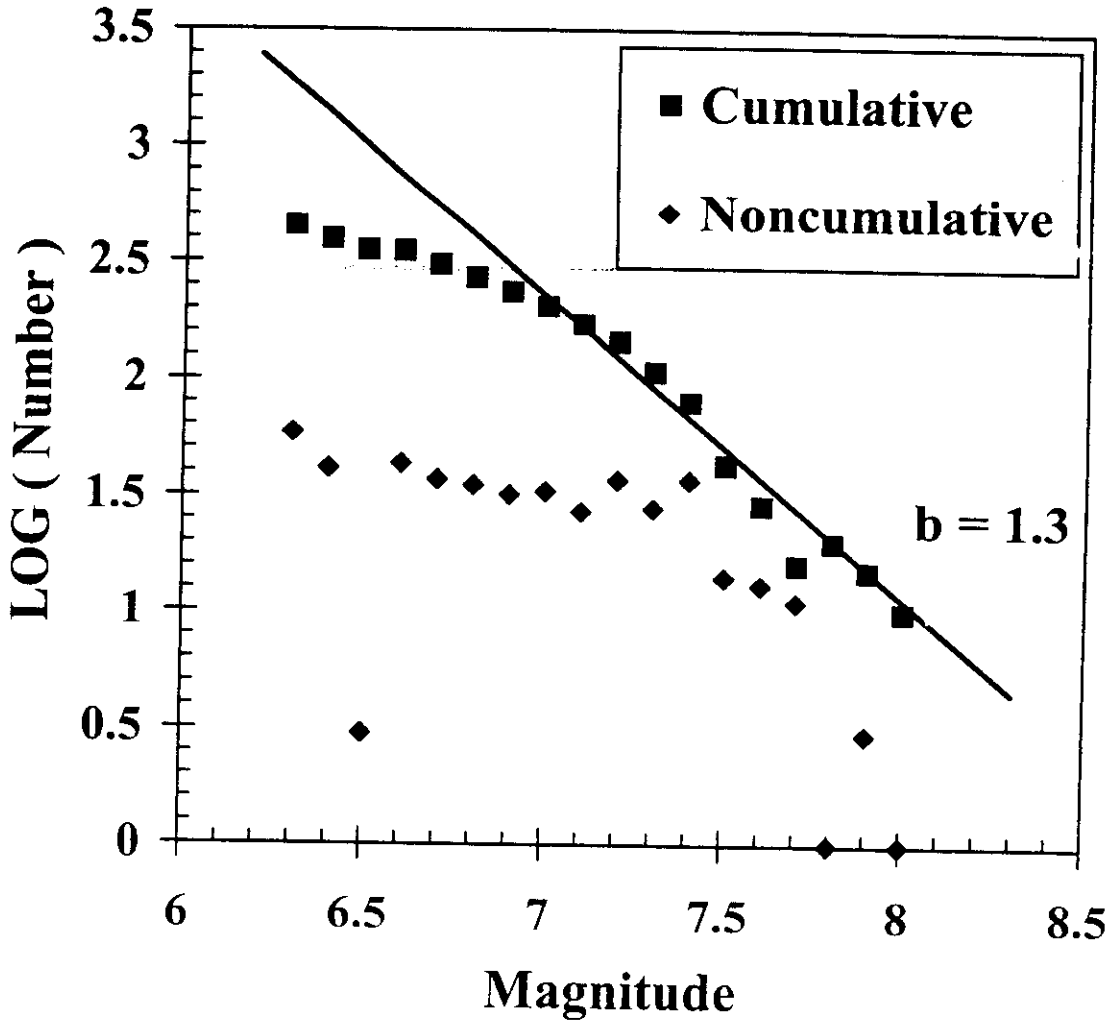
3.5
3
2.5
2
1.5
1
0.5
0
LOG (Number)
Cumulative
Noncumulative
b = 1.3
6
6.5
7
7.5
8
8.5
Magnitude

Fig. 12

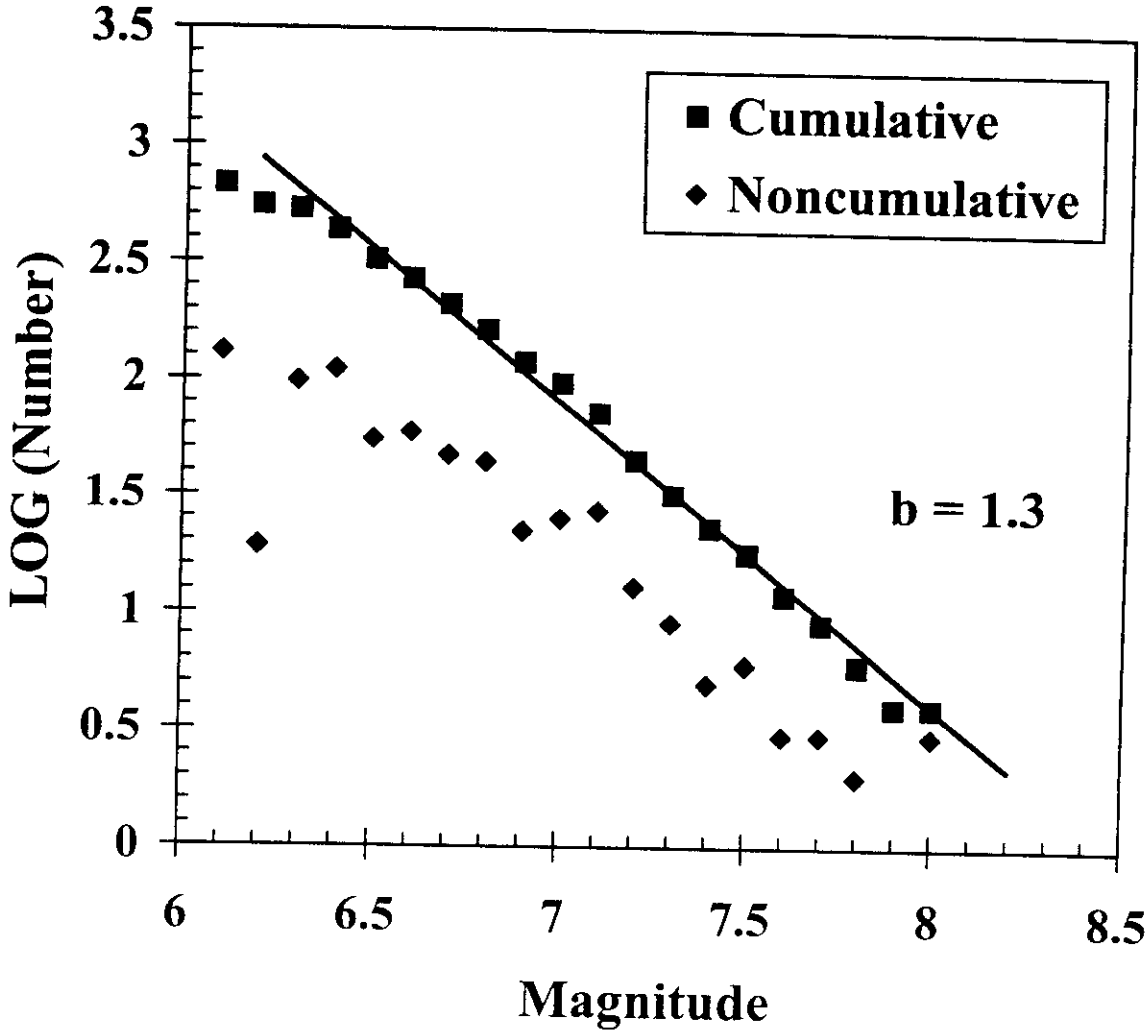
3.5
3
2.5
2
1.5
1
0.5
0
LOG (Number)
Cumulative
Noncumulative
b = 1.3
6
6.5
7
7.5
8
8.5
Magnitude

Fig. 13

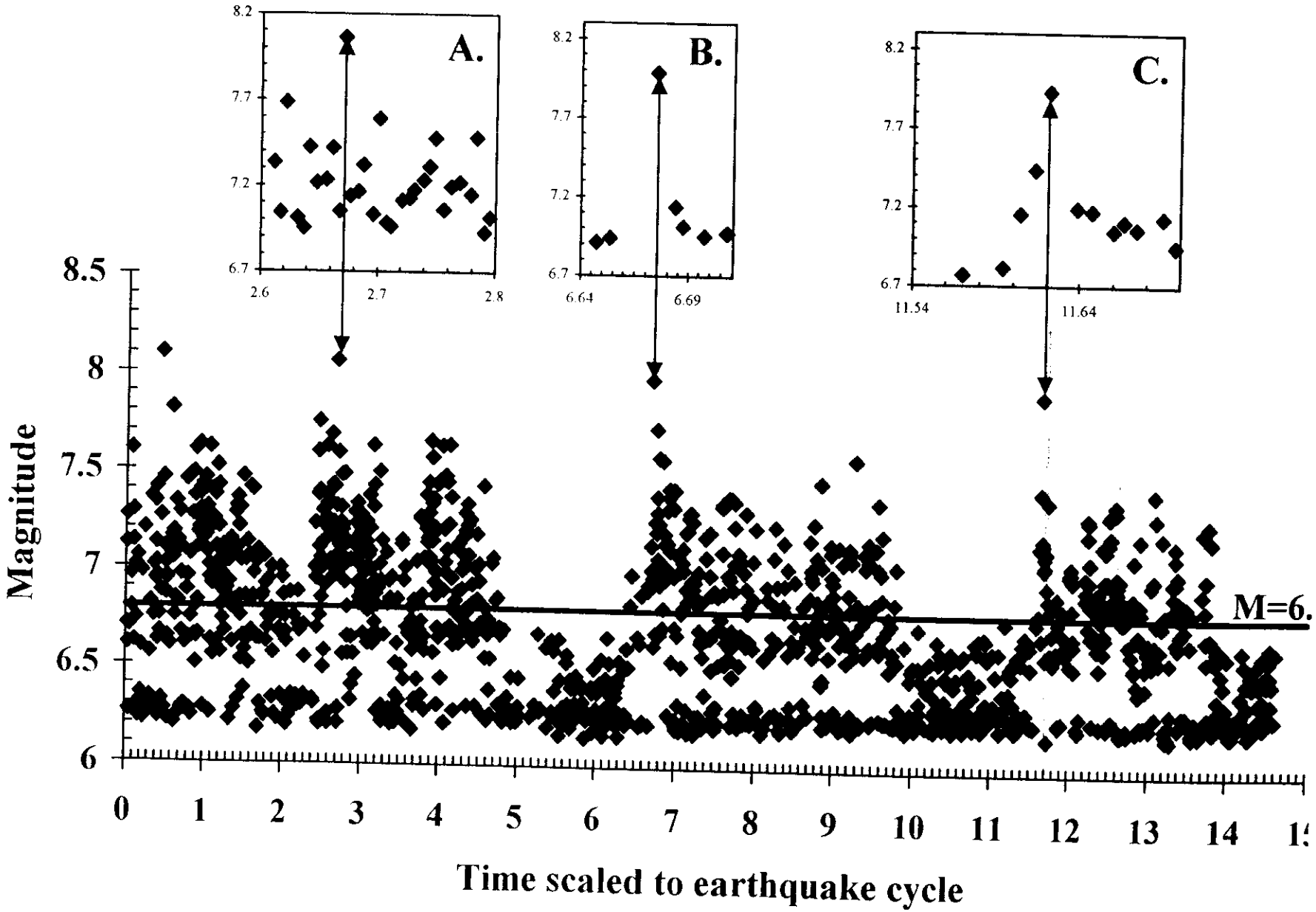
A.
B.
C.
8.2
7.7
7.2
6.7
2.6
2.7
2.8
6.64
6.69
11.54
11.64
8.5
8
7.5
7
6.5
6
Magnitude
M=6.
0
1
2
3
4
5
6
7
8
9
10
11
12
13
14
Time scaled to earthquake cycle

Fig. 14

Self-Driven Mode Switching of Earthquake Activity on a Fault System

Yehuda Ben-Zion*, Karin Dahmen†, Vladimir Lyakhovsky‡,
Deniz Ertas§, and Amotz Agnon^

* Dept. of Earth Sciences, Univ. of Southern CA, Los Angeles, CA, 90089-0740, USA. Phone: (1-213)-740-6734, fax: (1-213)-740-8801, email: benzion@terra.usc.edu (Corresponding Author.)

† Dept. of Physics, University of Illinois at Urbana Champaign, 1110 West Green Street, Urbana, IL 61801-3080, Phone: (1-217)-244-8873, fax: (1-217)-333-9819, email: dahmen@uiuc.edu

‡ Inst. of Earth Sciences, The Hebrew University, Jerusalem, Israel. Phone: (972-2)-658-4670, fax: (972-2)-566-2581, email: vladi@cc.huji.ac.il

§ Exxon Corporate Research Lab, Annandale, New Jersey, 08801, USA. Phone: (1-908)-730-2779, fax: (1-908)-730-3232, email: mdertas@erenj.com

^ Inst. of Earth Sciences, The Hebrew University, Jerusalem, Israel. Phone: (972-2)-658-4743, fax: (972-2)-566-2581, email: amotz@cc.huji.ac.il

Earth Planet. Sci. Lett., vol. 172/1-2, pp. 11-21, 1999

Keywords: earthquake dynamics, nonlinear dynamics, seismicity patterns

Abstract

Theoretical results based on two different modeling approaches indicate that the seismic response of a fault system to steady tectonic loading can exhibit persisting fluctuations in the form of self-driven switching of the response back and forth between two distinct modes of activity. The first mode is associated with clusters of intense seismic activity including the largest possible earthquakes in the system and frequency-size event statistics compatible with the characteristic earthquake distribution. The second mode is characterized by relatively low moment release consisting only of small and intermediate size earthquakes and frequency-size event statistics following a truncated power law. The average duration of each activity mode scales with the time interval of a large earthquake cycle in the system. The results are compatible with various long geologic, paleoseismic, and historical records. The mode switching phenomenon may also exist in responses of other systems with many degrees of freedom and nonlinear dynamics.

Introduction

Seismicity patterns are characterized by a variety of fluctuations including foreshocks, aftershocks, periods of quiescence, migration of earthquakes along fault zones, switching of activity among different faults, and more [1]. It is, however, usually assumed that over time scales longer than a few large earthquake cycles and shorter than geological periods (e.g., 10^3 yr $\leq$ time $\leq 10^6$ yr in tectonically active areas), regional and local statistics of earthquakes are stationary in time. The most common types of statistics used to describe seismicity patterns of tectonic earthquakes are temporal decay of aftershock rates, and frequency-size distribution of earthquakes giving relative frequencies of events in different size ranges. It is widely accepted that, to first order, aftershock rates are distributed according to the modified Omori power law [2] regardless of location or time. In contrast, the form of frequency-size statistics is a much debated subject. Kagan [3-5] analyzed regional and global earthquake catalogs and argued, based on these observations, that

frequency-size statistics of tectonic earthquakes follow everywhere the Gutenberg-Richter power law relation with a roughly universal exponent (b-value close to 1). On the other hand, Wesnousky [6-7] and others [8-9] examined statistics of earthquakes in various individual fault systems occupying narrow and long spatial domains. The results emerging from the latter studies, and related theoretical works [10-12], suggest that Gutenberg-Richter type statistics in individual fault zones are limited to immature structures with strong geometric disorder. In contrast, frequency-size earthquake statistics in relatively regular structures, associated with highly-slipped mature fault zones, are better described by a "characteristic earthquake" distribution, consisting of power law statistics of small events combined with strong enhancement in the frequency of earthquakes having a certain "preferred" size (see, e.g. the distribution at the bottom of region 2 in Figure 5a).

In this paper we present theoretical results, based on two different modeling approaches [13-14], which show that in certain parameter ranges models of individual fault systems can switch spontaneously their mode of seismic response to slow tectonic loading, from a time interval with frequency-size statistics following the characteristic earthquake distribution to an interval with Gutenberg-Richter statistics and back. In the intervals associated with the characteristic earthquake distribution the largest possible events in the system occur, while in the periods associated with the Gutenberg-Richter statistics there are only small and intermediate size earthquakes. The activity switching results from episodic global reorganization of the mode of strain energy release in the system, associated with a statistical competition between a tendency for a synchronized behavior and a tendency for a disordered response. These tendencies are approximately equal for the range of model parameters generating mode switching of activity. The persistence time in each mode is scaled by the time of a large earthquake cycle on the generating fault system. Thus, the observation of mode switching in natural seismicity requires long records containing many large earthquake cycles. Although data sets of such long duration are not very common, available paleoseismic [15-22], historical [23-24], and geological [25-26] observations (see

the "Discussion" section of the paper) indicate that mode switching of seismic activity of the type simulated here may occur in nature. The mode switching phenomenon can unify a variety of observations associated with the occurrence of earthquakes, some explained presently by separate frameworks and others unexplained as yet. On fault zones having mode switching activity, earthquake statistics are non-stationary on time scales shorter than several mode switching periods. This has important implications for seismic hazard assessment and other studies based on extrapolations of short duration data. The results may be relevant to other systems with many degrees of freedom and nonlinear dynamics.

Analysis

Figure 1 shows a regional lithospheric model consisting of a seismogenic upper crust governed by damage rheology over a Maxwell viscoelastic substrate [13]. The model calculates the coupled evolution of earthquakes and faults in a framework incorporating damage rheology compatible with observed nonlinear and irreversible features of strain, and essential 3-D aspects of lithospheric deformation. The damage rheology, discussed in detail by Lyakhovsky et al. [27], has two types of functional coefficients: (1) a "generalized friction coefficient" separating states associated with material degradation and healing, and (2) damage rate coefficients for positive (degradation) and negative (healing) changes. The evolving damage modifies the effective elastic properties of material in the seismogenic zone as a function of the ongoing deformation. This simulates the creation, evolution, and possible healing of fault systems in the upper brittle crust. The seismogenic zone is coupled viscoelastically to the substrate, where steady plate motion drives the lithospheric deformation. The viscous crustal deformation is calculated using variables that are vertically averaged over the crust thickness (H+h in Figure 1), while the elastic deformation is calculated with a 3-D Green function for elastic half-space. Lyakhovsky et al. [13] provide a detailed description of the simulation procedure and a large parameter-space study. Here we focus on results relevant to mode switching of seismic activity.

Figure 2 shows map views of simulated damage in the upper crust at different times, illustrating the evolution of fault zones in the regional lithospheric model of Lyakhovsky et al. [13]. The boundary conditions and large scale geometrical, rheological, and damage parameters used to generate Figure 2 are indicated in Figure 1 and the inset of Figure 3. The assumed parameter values for the upper crust (thickness H, rigidity for zero damage μ_0, generalized friction coefficient ξ_0, Poisson's ratio ν), lower crust (thickness h, viscosity η, rigidity μ_a, Poisson's ratio ν), and imposed plate motion at the base of the lower crust, were determined by fitting model calculations to average observed geodetic deformation associated with the San Andreas fault in California, and additional regional constraints from observed seismological and geodetic data [13]. The key remaining parameter is the ratio of time scale for damage healing (τ_H) to time scale for loading (τ_L). Each brittle model event is associated with abrupt strength degradation and abrupt stress drop. The value of τ_H depends on the damage rate coefficients for healing and it controls the time for strength recovering after the occurrence of a brittle event. The value of τ_L depends on the boundary conditions and large scale parameters (which determine also the average time of a large earthquake cycle) and it controls the time for re-accumulation of stress at a failed location. Relatively high ratios of τ_H/τ_L (top curve in the inset of Figure 3) lead to the development of geometrically regular fault zones and frequency-size event statistics compatible with the characteristic earthquake distribution. Relatively low ratios of τ_H/τ_L (bottom curve in the inset of Figure 3) lead to the development of highly disordered fault zones and frequency-size statistics compatible with the Gutenberg-Richter distribution. Lyakhovsky et al. [13] illustrate and discuss these results.

The evolving fault (damage) zones of Figure 2 and associated seismicity patterns (Figure 3) are generated for intermediate ratios of τ_H/τ_L around the middle line in the inset of Figure 3, small uncorrelated random noise in the spatial distribution of ξ_0, and the large scale parameters of Figure 1. Remarkably, for such cases the evolving fault zones maintain a level of geometrical disorder similar to those present in the last three frames of Figure 2, and

the seismic response of the model alternates between time intervals of intense seismic activity containing clusters of large events, and lower activity periods during which only small to moderate earthquakes occur (Figure 3). The time interval of each mode of activity scales with the average repeat time of large model earthquakes in the more active periods. During the low activity intervals the rate of strain energy release in the crust is lower than the rate of energy accumulation from loading, while during the high activity intervals the opposite is true. The model alternates between these two modes, rather than settling on a steady response with energy release rate equal the rate of energy accumulation. The frequency-size statistics of earthquakes in the intervals with and without clusters of large events are compatible approximately with the characteristic earthquake and Gutenberg-Richter distributions, respectively. The mode switching results are somewhat surprising and they may appear at first as having only a limited value associated with a curious dynamic behavior. However, as we show below, very similar behavior is seen in an independent theoretical analysis and observed earthquake and fault data.

Figure 4 shows a model for an individual strike-slip fault system without damage evolution in a 3-D half-space [10-12, 14, 28]. This much simpler model contains a computational grid where evolving seismicity patterns are generated in response to ongoing loading imposed as slip boundary conditions on the other fault regions. The brittle properties of the computational grid are characterized by static strength threshold and arrest stress distributions that are spatially heterogeneous but fixed in time, and a dynamic weakening coefficient ε. The latter simulates a reduction from static friction to dynamic strength at a point on a fault sustaining multiple slip episodes during a given model earthquake [10]. The stress transfer along the fault due to the imposed boundary conditions and failure episodes in the computational grid is calculated with a "mean field" Green function [28, 14] that replaces the actual elastic stress response to dislocations [10-12] with a constant value. The mean field Green function can not be used to calculate details of deformation fields or other specific phenomena, but it provides an appropriate tool for

studying questions such as possible types and exponents of statistics characterizing event populations generated under different conditions [29].

Dahmen et al. [14] mapped the dynamics of this fault system onto a phase diagram (Figure 5a) spanned by the dynamic weakening coefficient ε and a conservation parameter c related to dissipation of stress transfer and the size of the system. The values of ε range from 0 at no weakening (dynamic friction equal static friction) to 1 at complete weakening (dynamic friction equal 0). The values of c range from 0 at complete dissipation (corresponding here to the unphysical case of a fault that is loaded, in addition to the boundary conditions on the continuation of the computational grid, directly at the rupture zone) to 1 at complete conservation of stress transfer (corresponding to the physical case of a fault loaded by motion of tectonic plates far away and deformation of the surrounding material). At exactly $\varepsilon = 0$ and $c = 1$ there is a critical point of a second order phase transition [28] and the frequency-size distribution of simulated model earthquakes is given by the Gutenberg-Richter power law relation. If ε and c belong to region 1 of the phase diagram, the frequency-size statistics consist of a truncated power law, a form generally compatible with the Gutenberg-Richter distribution. Remarkably, we find also here that for a range of dynamic weakening and dissipation parameters that map into the more physical region 2, the seismicity (Figure 5b, top) switches spontaneously back and forth, as in the model of Lyakhovsky et al. [13], between time periods containing large events following the characteristic earthquake distribution, and time periods containing only small to moderate earthquakes following a truncated power law distribution.

As discussed by Dahmen et al. [14], the activity switching in this model results from episodic global reorganization of the mode of strain energy release of the fault system, reflected in the configurational entropy of stress states on the fault (Figure 5b, bottom). This is associated with a statistical competition between a tendency for a synchronized behavior leading to clusters of large earthquakes and the characteristic earthquake distribution, and a tendency for disordered response leading to Gutenberg-Richter type statistics without a

preferred event size. For model parameters in region 2 of Figure 5a, these two opposite tendencies are roughly equal in strength. A similar dynamic mechanism probably generates the alternating "undershoot" and "overshoot" responses in the regional model of Lyakhovsky et al. [13].

Discussion

We study long histories of simulated seismicity patterns using two separate frameworks. The first, more realistic model [13], employs a lithospheric domain with regional seismogenic zone governed by damage rheology, viscoelastic substrate, multiple evolving faults, and 3-D elastic Green function for stress transfer due to brittle failures. The second, simpler model [14], simulates seismicity on a single fault system with prescribed planar geometry, elementary rheology, and a mean field approximation of the stress transfer function. The more realistic framework can address a much broader class of questions than the simpler model can. However, this is somewhat compensated by a greater ability of the simpler model to obtain a basic understanding of common underlying dynamic mechanisms. In both cases, we find that the models generate for ranges of parameters self-driven mode switching of seismic activity. The actual mode switching times are statistical events and the average persistence time for each mode, in the more realistic model [13], is on the order of a few large earthquake cycles. Examples of large earthquake cycles on major natural active fault zones are hundreds of years for the San Andreas fault and thousands of years for the Dead sea transform in Israel. Thus, observational confirmation of response switching on large fault systems of the type predicted by our models requires data sets that are many thousands of years long.

Marco et al. [15] compiled from slip and damage events in sediments of the Lisan lake in the Dead sea region, Israel, a 50 kyr history of moderate and large ($M \geq 6$) earthquakes occurring along the Dead sea transform in that area. Their obtained paleoseismic data consist of alternating time intervals, on the order of 5-10 kyr each (i.e., a

few large earthquake cycles), with distinctly different seismic character. In half of the intervals the sedimentary record contains clear signatures of moderate to large events, while in the other half very few or no such signatures exist. Leonard et al. [16] performed a Bayesian statistical analysis of a 50 kyr long paleoseismic earthquakes along the Arava segment of the Dead sea transform, approximately 100 km south of the study area of ref. [15]. The data sets of refs. 15-16 overlap only partially in time and span together about 70 kyr. Leonard et al. [16] concluded that there was a clear change in the seismic behavior of the Arava fault around 15 kyr ago. In the interval 15-35 kyr ago (a period overlapping with the most recent cluster of intense seismic activity in the data of Marco et al. [15]), the statistical analysis of earthquakes on the Arava fault favors the characteristic earthquake distribution. In contrast, the frequency-size statistics of earthquakes occurring on that fault in the last 15 kyr are compatible with either the Gutenberg-Richter distribution or a characteristic earthquake distribution with a smaller characteristic earthquake magnitude. Ambraseys and others [17-19] assembled long earthquake histories for the North and East Anatolian faults in Turkey and other faults in the Middle East. Their complied earthquake histories show, like the Dead sea transform, alternating periods of activity with and without moderate to large earthquakes. There is recent evidence for similar mode switching on the Altyn Tagh fault in China [20]. These fluctuations of earthquake activity, which until now were unexplained, appear to reflect mode switching of the seismic response of individual large fault systems, as seen in our model calculations. It is difficult to explain these observations by other mechanisms, such as interaction with near-by large faults, since the Dead sea transform, North Anatolian, East Anatolian, and Altyn Tagh faults are each the only major fault system in the associated tectonic domain.

Other data sets are also compatible with the mode switching of seismic activity discussed in this work. These include episodic clusters of large historic earthquakes in the middle east [23] and east Asia [24], evidence for several widely separated periods with and without large earthquakes in the new Madrid, eastern US, seismic zone [22], changes in the

character of activity along several faults in the basin and range, western US, province [25], episodic clustering of activity in the last 10 kyr years along fault segments in the rupture zone of the 1992 Landers, CA, earthquake [21], and geologic data combined with recent geodetic and seismological measurements showing changes in the character of accumulation and release of seismic energy on the San Miguel fault, Mexico [26]. Some of the latter observations may result from other physical mechanisms or incompleteness of data. However, such explanations can not hold for all the discussed data, especially those associated with the Dead sea transform, North Anatolian, East Anatolian, and Altyn Tagh faults.

An extreme manifestation of mode switching of seismic activity may produce transitions between brittle (seismic) and effectively creeping (or aseismic) responses to tectonic loading. It is interesting to speculate that the currently creeping segment of the central San Andreas fault had in the past (and may have in the future) large earthquake ruptures. If so, paleoseismic trenching may provide evidence for past large earthquakes in the creeping segment, and seismological, geodetic, and other imaging methods may show signatures of locked fault zone structures. We note that Eberhart-Phillips and Michael [30] pointed out, based on seismic tomography of the central San Andreas fault, that the velocity structure along part of the creeping segment is similar to that of the locked section associated with the rupture zone of the great 1857 earthquake.

Conclusions

The debate on the form of frequency-size statistics of earthquakes has been polarized so far [4-12] into either the Gutenberg-Richter or characteristic earthquake distributions but not both. The theoretical and observational results discussed in this paper indicate that the seismic behavior of a fault system can change spontaneously from response following one type of statistics to the other. In places where such mode switching occurs, the time scale over which the seismicity may be regarded as stationary is at least several

times larger than the persistence time in each mode, e.g. 5-10 kyr for the San Andreas fault and 50-100 kyr for the Dead sea transform. These results have far reaching implications for the overall understanding of earthquake and fault dynamics, and various specific applications such as seismic hazard assessment. We note that fluctuations similar to our mode switching results may be present in behavior of other systems with many degrees of freedom and nonlinear dynamics, such as communication networks [31]; climate [32], and the Earth magnetic field [33].

Acknowledgments

We thank Geoff King, Andy Michael, Phil Pollett, and Rick O'Connell for useful Comments. The research was supported by the National Science Foundation (grant EAR-9725358) and the Southern California Earthquake Center (based on NSF Cooperative Agreement EAR-8920136 and USGS Cooperative Agreement 14-08-0001-A0899).

References

1. Simpson, D. W. and P. G. Richards, eds., Earthquake prediction, American Geophysical Union, Washington, DC, 1981, 680 pp.
2. Utsu, Y., Y. Ogata, and R. S. Matsu'uara, The centenary of the Omori formula for a decay law of aftershock activity, J. Phys. Earth, 43 (1995) 1-33.
3. Kagan, Y. Y., Observational evidence for earthquakes as a nonlinear dynamic process, Physica D, 77 (1994) 160-192.
4. Kagan, Y. Y. Comment on "The Gutenberg-Richter or characteristic earthquake distribution, which is it?" by Wesnousky [1994], Bull. Seismol. Soc. Amer., 86 (1996) 274-285.
5. Kagan, Y. Y., Seismic moment-frequency relation for shallow earthquakes: Regional comparison, J. Geophys. Res., 102 (1997) 2835-2852.

6. Wesnousky, S. G., The Gutenberg-Richter or characteristic earthquake distribution, which is it?, Bull. Seismol. Soc. Amer., 84 (1994) 1940-1959.

7. Wesnousky, S. G., Reply (to comment by Kagan), Bull. Seismol. Soc. Amer., 86 (1996) 285-291.

8. Stirling, M. W., S. G. Wesnousky and K. Shimazaki, Fault trace complexity, cumulative slip, and the shape of the magnitude-frequency distribution for strike-slip faults: a global survey, Geophys. J. Int., 124 (1996) 833-868.

9. Schwartz, D. P. and K. J. Coppersmith, Fault behavior and characteristic earthquakes: Examples from the Wasatch and San Andreas fault zones, J. Geophys. Res., 89 (1984) 5681-5698.

10. Ben-Zion, Y. and J. R. Rice, Earthquake failure sequences along a cellular fault zone in a 3D elastic solid containing asperity and nonasperity regions, J. Geophys. Res., 98 (1993) 14109-14131.

11. Ben-Zion, Y. and J. R. Rice. Slip patterns and earthquake populations along different classes of faults in elastic solids, J. Geophys. Res., 100 (1995) 12959-12983.

12. Ben-Zion, Y., Stress, slip and earthquakes in models of complex single-fault systems incorporating brittle and creep deformations, J. Geophys. Res., 101 (1996) 5677-5706.

13. Lyakhovsky, V., Y. Ben-Zion and A. Agnon, Earthquake cycle, fault zones and seismicity patterns in a rheologically layered lithosphere, submitted to J. Geophys. Res., (1999).

14. Dahmen, K., D. Ertas and Y. Ben-Zion, Gutenberg Richter and Characteristic Earthquake behavior in Simple Mean-Field Models of Heterogeneous Faults, Phys. Rev. E, 58 (1998) 1494-1501.

15. Marco, S., M. Stein, A. Agnon and H. Ron, Long term earthquake clustering: a 50,000 year paleoseismic record in the Dead sea graben, J. Geophys. Res., 101 (1996) 6179-6192.

16. Leonard G., D. M. Steinberg, and N. Rabinowitz, An indication of time-dependent seismic behavior - an assessment of paleoseismic evidence from the Arava fault, Israel, Bull. Seismol. Soc. Amer., 88 (1998) 767-776.

17. Ambraseys N. and Finkel C., The seismicity of Turkey, Eren Press, Istanbul, 1995, 240 pp.

18. Ambraseys N and Melville C., A history of Persian earthquakes, Cambridge University Press, London, 1982.

19. Ambraseys N, Melville C. and Adams R., Seismicity of Egypt, Arabia and the Red Sea, Cambridge University Press, London, 1994.

20. Geoffrey King, per communication, 1998.

21. T. K. Rockwell, S. Lindvall, M. Herzberg, D. Murbach, T. Dawson, and G. Berger, Paleoseismology of the Johnson Valley, Kickcapoo and Homestead Valley faults of the Eastern California Shear Zone, Bull. Seismol. Soc. Amer., in review (1999).

22. Sexton, J. L. and P. B. Jones, Evidence for recurrent faulting in the New Madrid seismic zone, Geophysics, 31 (1986) 1760-1788.

23. Nur, A. and E. H. Cline, Plate tectonics, earthquake storms, and system collapse at the end of the late bronze age in the Aegean and eastern Mediterranean, J. of Archaeological Science, in press (1999).

24. Kyung, J. B., K. Oike, and T. Hori, Temporal variations in seismic and volcanic activity and relationship with stress field in east Asia, Tectonophysics, 267 (1996) 331-342.

25. Wallace, R. E., Grouping and migration of surface faulting and variations in slip rates on faults in the great basin province, Bull. Seismol. Soc. Amer., 77 (1987) 868-876.

26. Hirabayashi, C. K., T. K. Rockwell, S. G. Wesnousky, M. W. Stirling, and F. Suarez-Vidal, A Neotectonic study of the San Miguel–Vallecitos Fault, Baja California, Mexico, Bull. Seismol. Soc. Amer., 86 (1996) 1770-1783.

27. Lyakhovsky, V., Y. Ben-Zion and A. Agnon, Distributed Damage, Faulting, and Friction, J. Geophys. Res., 102 (1997) 27635-27649.

28. Fisher, D. S., K. Dahmen, S. Ramanathan and Y. Ben-Zion, Statistics of Earthquakes in Simple Models of Heterogeneous Faults, Phys. Rev. Lett., 78 (1997) 4885-4888.

29. Ma, S. K., Modern Theory of Critical Phenomena, Benjamin, 1976 (and references therein).

30. Eberhart-Phillips, D. and A. J. Michael, Three-dimensional velocity structure and seismicity in the Parkfield region, central California, J. Geophys. Res., 98 (1993) 15,737-15,758.

31. Gibbens, R. J., Hunt, P. J. and Kelly, F. P., Bistability in communication networks. In "Disorder in Physical Systems" (Eds. G.R. Grimmett and D.J.A. Welsh), Oxford University Press, (1990) 113-127.

32. Appenzeller, C., T. F. Stocker and M. Anklin, North Atlantic oscillation dynamics recorded in Greenland ice cores, Nature, 283 (1998) 446-449.

33. Lund, S. P., G. Acton, B. Clement, M., Hastdt, M. Okada, T. Williams and others, Geomagnetic field excursions occurred often during the last million years, EOS Trans. Amer. Geophys. Union, 79 (1998) 178-179.

Figure Captions

Figure 1. Geometry and parameters for the model of ref. 13 simulating the coupled evolution of earthquakes and faults. The crust consists of a brittle seismogenic zone governed by damage rheology over a viscoelastic lower crust driven by steady mantle motion from below. H and h mark thickness of upper and lower crust layers, respectively. Parameters μ, ξ, η, and ν denote rigidity, generalized friction coefficient, viscosity, and Poisson's constant, respectively. The viscosity of the mantle is much larger than that of the lower crust. The instantaneous response of the entire model to brittle deformation in the upper crust in governed by a Green function for a 3-D elastic

half-space. The boundary conditions are constant stress at the left and right edges and periodic repeats at the front and rear boundaries.

Figure 2. Map views of damage distribution at four snapshots for damage healing time scale following the middle curve in the inset of Figure 3 (where we show the associated seismic record). The model is initiated with random damage distribution peaked at about α=0.5. The damage does not change significantly in the first few large earthquake cycles, during which elastic strains build up and the rate of material degradation grows at locations of damage (and strain) concentration. After this transient period, at time t/T = 3 with T denoting average time of a large earthquake cycle, the damage localizes to a single major disordered fault zone with a large (30 km) gap and related complications in the lower part of the model. The gap is bounded by conjugate (right lateral) faults 20-30 km long. A 10 km step-over (dilatational jog) develops at the middle portion of the model. At t/T = 5 the gap narrows (20 km) and the overall structure is smoother. At that time the overall damage amplitude is generally lower than that of the previous panel. As shown in the related Figure 3, this period is an intermediate interval of low seismicity between clusters of higher activity. Some high damage zones that were previously active are healed and can hardly be recognized. At t/T = 7 an almost continuous disordered fault zone is established with two conjugate stepovers (dilatational and compressional). This stage represents an activation of a new cluster of high seismic activity. Further structural evolution cycles between patterns similar to those of the last three panels.

Figure 3. A long record of model earthquakes showing mode switching of seismic response in time. The seismic activity consists of cluster periods lasting a few large earthquake cycles, separated by relatively quiet intervals of similar length. During the cluster periods, the largest possible events in the system occur, the frequency-size event statistics are compatible with the characteristic earthquake distribution, and the overall moment release is an order of magnitude higher than the inter cluster periods. In the latter intervals there are only small and intermediate size earthquakes and the frequency-

size statistics follow approximately the Gutenberg-Richter distribution. The inset shows damage evolution for different ratios of τ_H/τ_L, where τ_H is characteristic time for damage healing and τ_L is characteristic loading time. The upper line is associated with relatively high ratio of τ_H/τ_L. For such a case the damage localizes to a simple major fault zone and the frequency-size statistics follow the characteristic earthquake distribution. The bottom line is associated with relatively low ratio of τ_H/τ_L. For this case the model generates a disordered network of faults and power law frequency-size statistics. For intermediate ratios of τ_h/τ_l around the middle line, the model produces a disordered major structure as in Figure 2 and the seismic response exhibits mode switching of activity as shown here.

Figure 4. Top: A schematic representation of an individual strike-slip fault system with a 3-D geometric disorder. Bottom: A simple representation of the 3-D disordered fault system by a 2-D fault embedded in a 3-D half-space. Each fault location (x, y = 0, z) represents deformation in a volume centered on the line (x, y, z). The geometric disorder is modeled as disorder in strength properties of the planar fault. The rectangular section is a computational grid where black and white patches denote locations of relatively high and relatively low stress thresholds to failure. The other fault regions creep at constant velocity. (Modified from ref. 12.)

Figure 5a. Phase diagram of simulated frequency-size earthquake statistics as a function of conservation of stress transfer c and dynamic weakening coefficient ε. A value $c = 1$ corresponds to a fault loaded from a "far-field" edge of a large spatial domain with no loss of stress transfer, whereas $c < 1$ corresponds to loading from the edge of a small spatial domain or the existence of a loss mechanism. A value $\varepsilon = 0$ corresponds to static friction only, whereas $\varepsilon > 0$ corresponds to the existence of both static and kinetic friction levels. Models with parameter values in region 1 can only produce Gutenberg-Richter (GR) types of statistics. Models in the more realistic region 2 can produce both Gutenberg-Richter and characteristic earthquake (CE) types of statistics. In such cases,

a finite fault will produce one type of statistics for a certain persistence time and then spontaneously switch to another mode in which it produces the other type. (Modified from ref. 14.)

Figure 5b. Sample time series of earthquake sizes (top) and corresponding configurational entropy (bottom). The model time t is given in units of the average repeat time T of the largest earthquakes in the characteristic earthquake phase. The earthquake size is given in units of rupture area. The top panel shows that after switching at t/T ≈ 3800 from the Gutenberg-Richter phase with mostly small earthquakes to the characteristic earthquake phase with quasi-periodically recurring large earthquakes and only very small earthquakes in between, the fault remains in the characteristic earthquake phase for roughly 4200 T before it spontaneously switches back into the Gutenberg-Richter phase. The configurational entropy is defined as the entropy of the distribution of stresses along the fault and is computed as a function of time. Large entropy implies large variations of stress states on the fault. Such stress states produce Gutenberg-Richter type of statistics. Small entropy indicates synchronization and a narrow distribution of stress states. In this case all parts of the fault tend to rupture together in one large event, in which they simultaneously release their stresses. Subsequently, different parts of the fault get reloaded more-or-less simultaneously (while producing only very few small earthquakes), until another large earthquake relaxes the entire fault and the cycle repeats, thereby producing characteristic earthquake type of statistics. (Modified from ref. 14.)

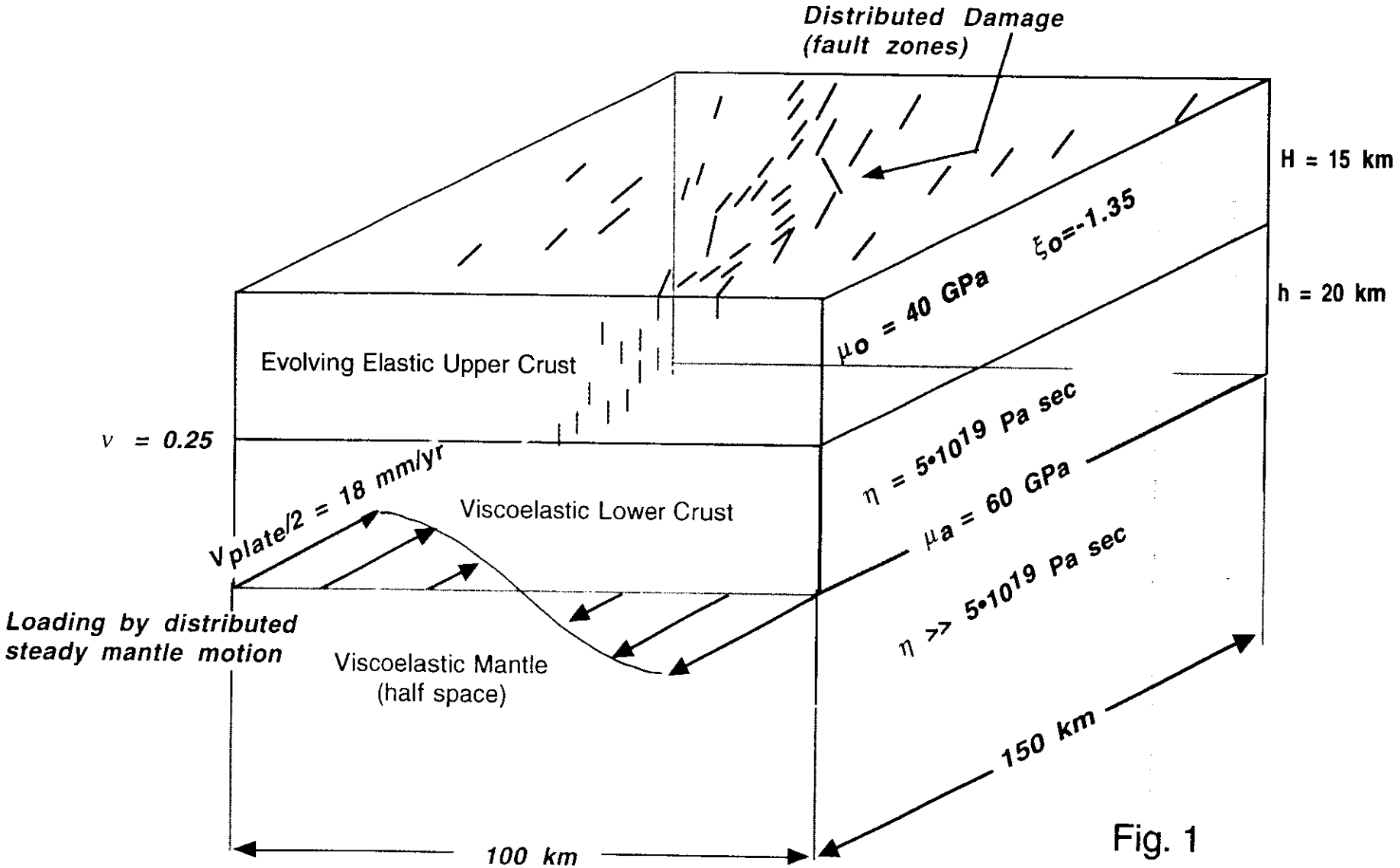
Distributed Damage
(fault zones)
H = 15 km
h = 20 km
ξo=-1.35
μo = 40 GPa
Evolving Elastic Upper Crust
ν = 0.25
η = 5•10^19 Pa sec
μa = 60 GPa
Vplate/2 = 18 mm/yr
Viscoelastic Lower Crust
Loading by distributed
steady mantle motion
η >> 5•10^19 Pa sec
Viscoelastic Mantle
(half space)
150 km
100 km

Fig. 1

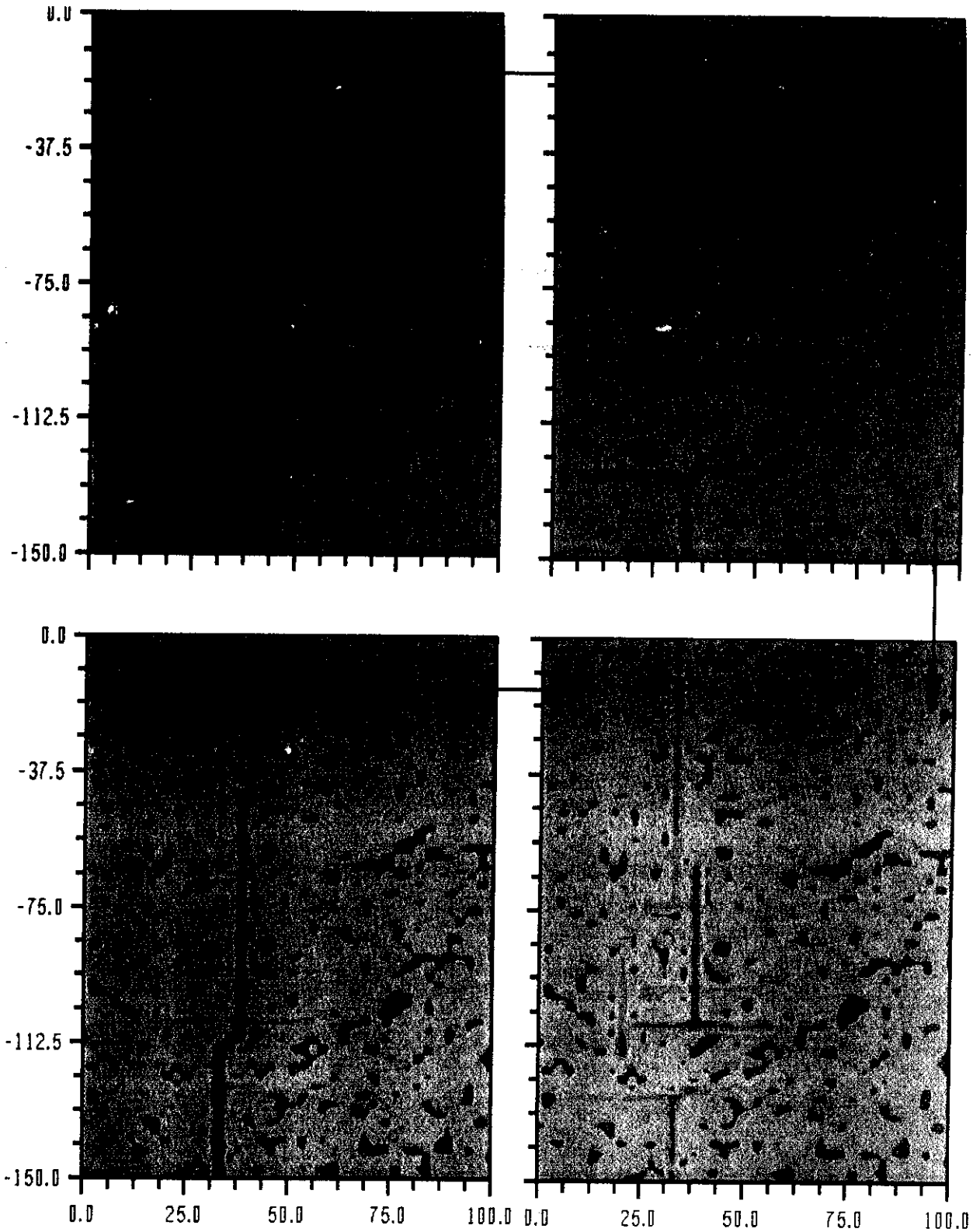

Damage (α)

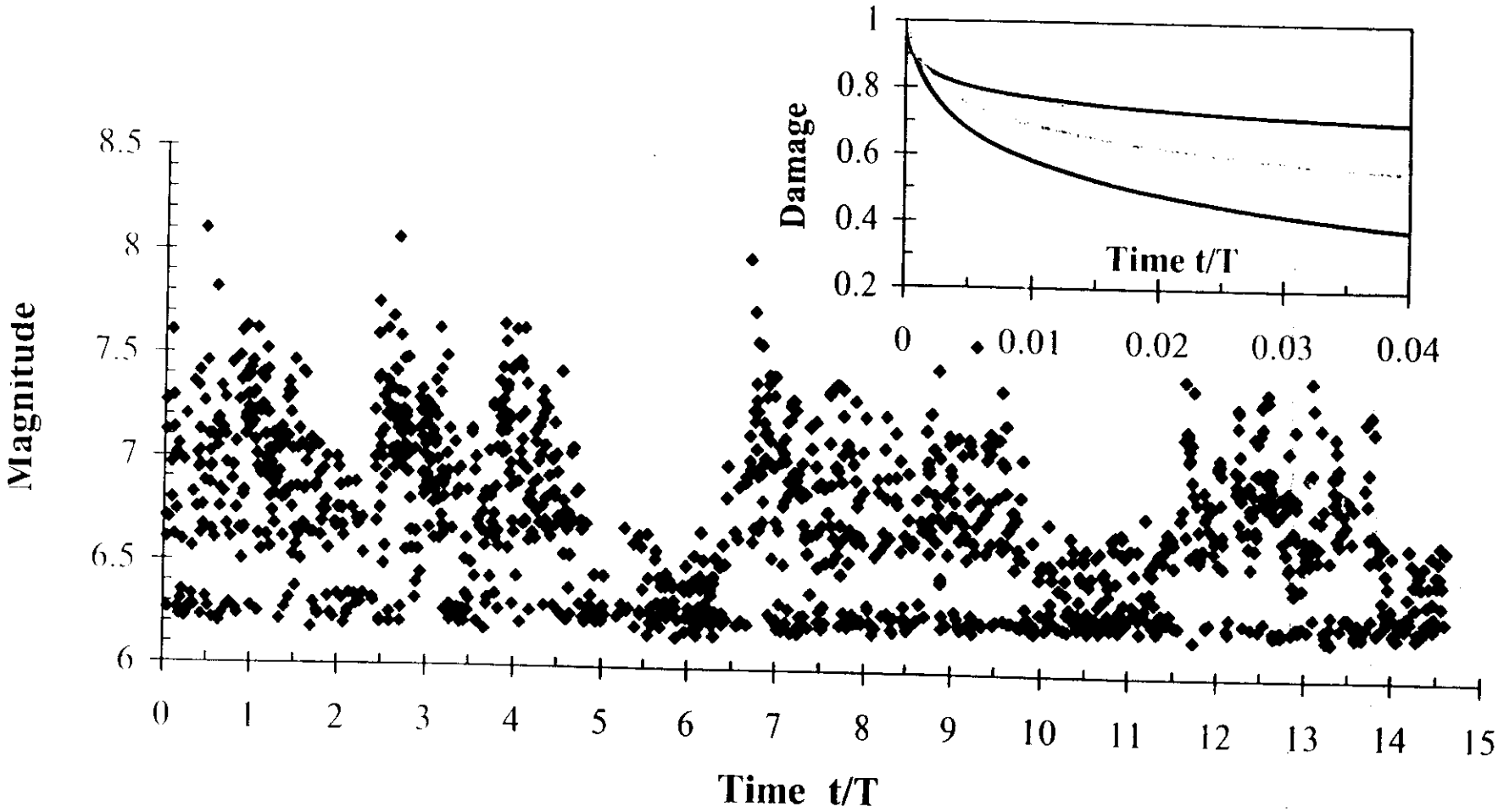
Magnitude
8.5
8
7.5
7
6.5
6
0 1 2 3 4 5 6 7 8 9 10 11 12 13 14 15
Time t/T
Damage
1
0.8
0.6
0.4
0.2
0 0.01 0.02 0.03 0.04
Time t/T

Fig. 3

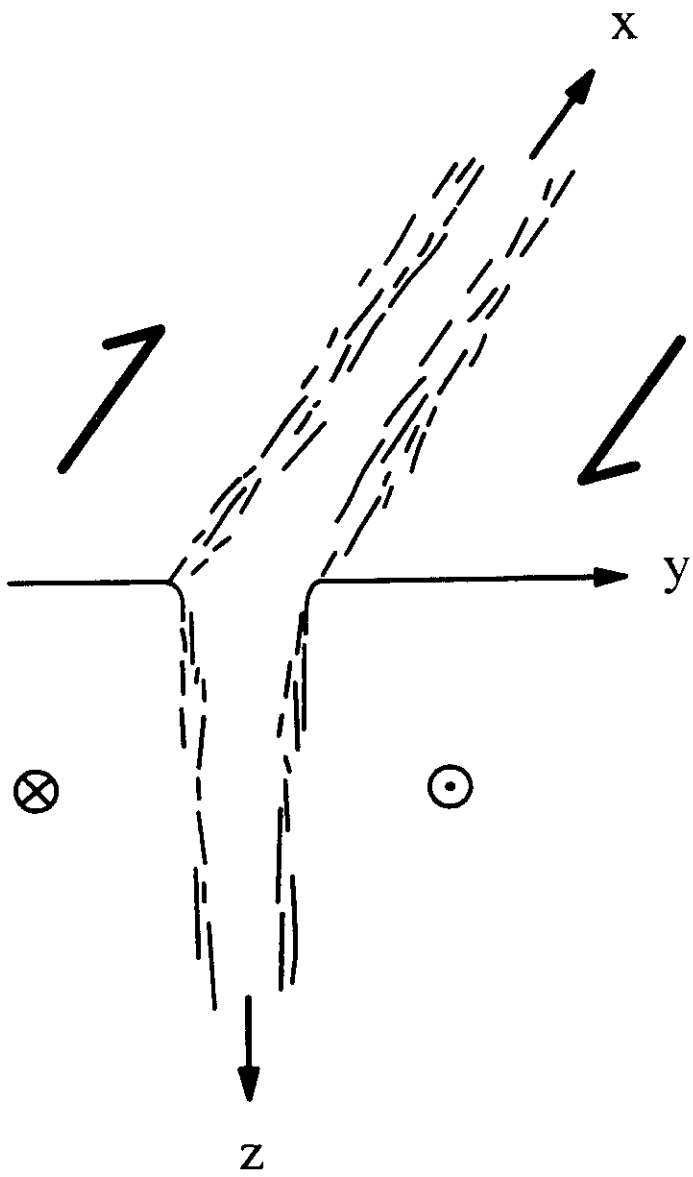
x
y
z

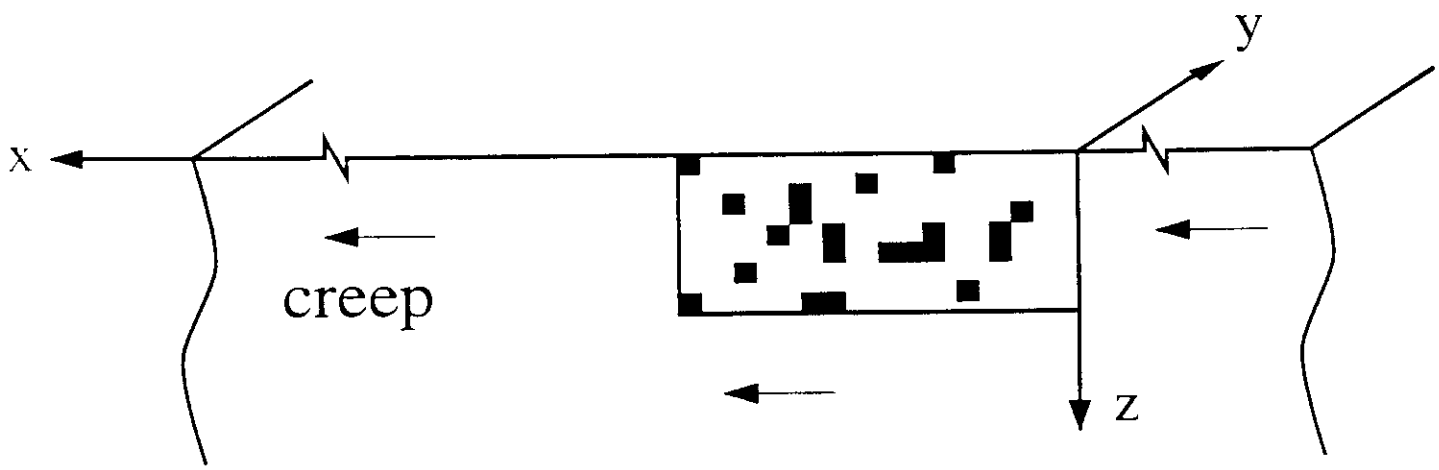
y
x
creep
z

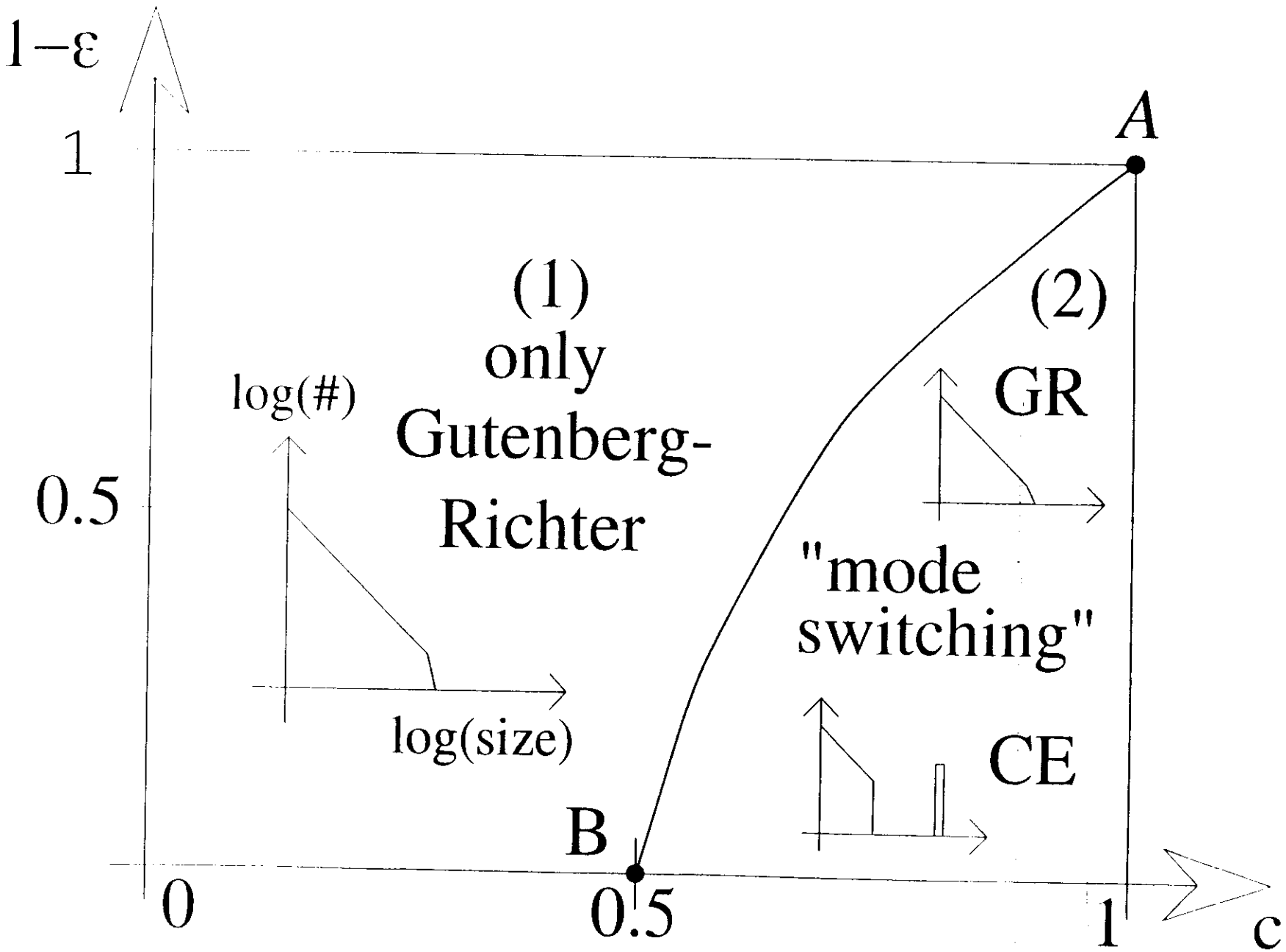
1−ε
1
0.5
0
0.5
1
c
A
B
(1)
only
Gutenberg-
Richter
log(#)
log(size)
(2)
GR
"mode
switching"
CE

Fig. 5a

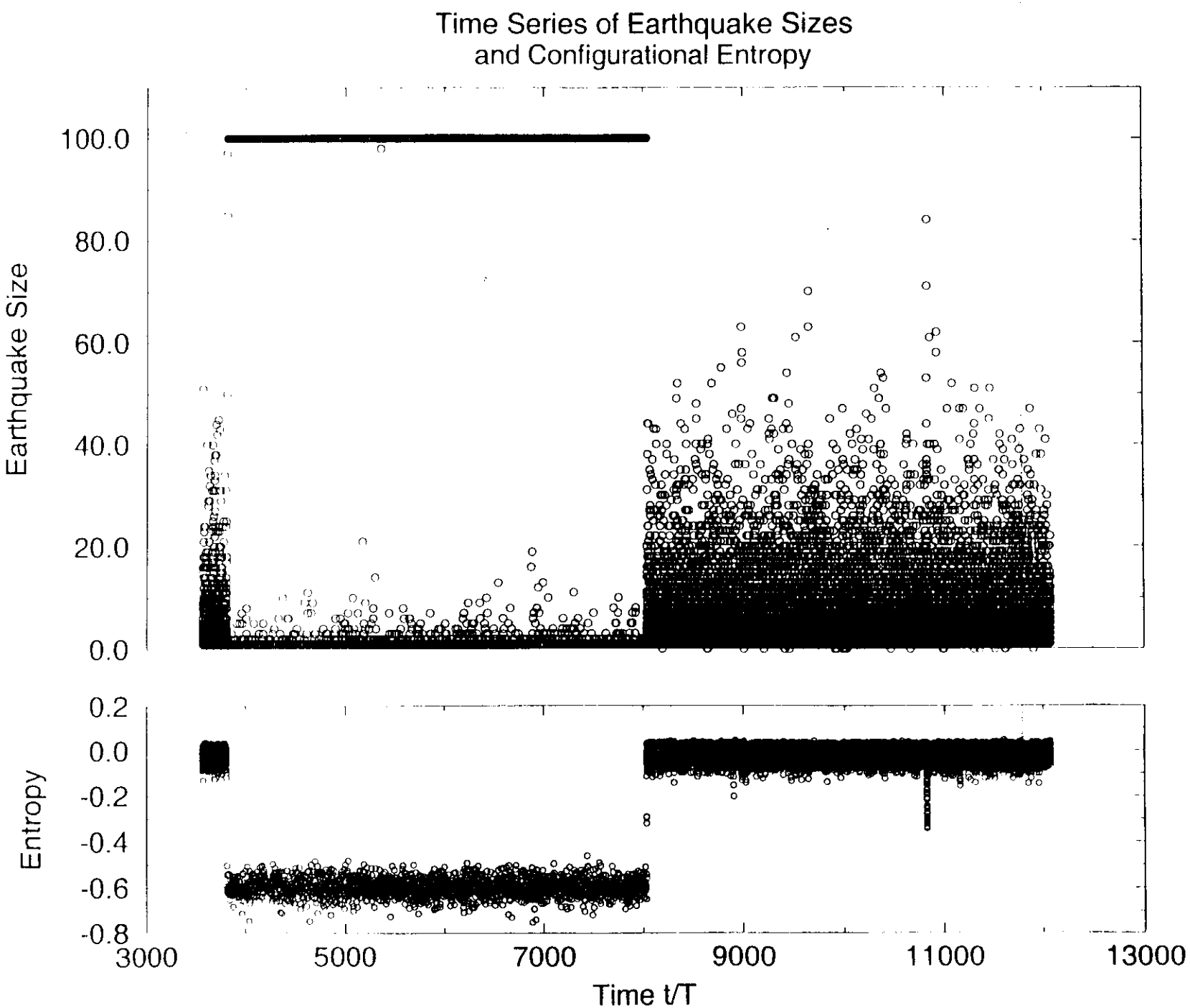
Time Series of Earthquake Sizes
and Configurational Entropy
Earthquake Size
100.0
80.0
60.0
40.0
20.0
0.0
Entropy
0.2
0.0
-0.2
-0.4
-0.6
-0.8
3000
5000
7000
9000
11000
13000
Time t/T

Fig 5b.